

Reexamining the potential to classify lava flows from the fractality of their margins

E. I. Schaefer^{1,2}, C. W. Hamilton³, C. D. Neish^{1,2}, M. M. Sori⁴, A. M. Bramson⁴, and S. P. Beard⁵

¹ Department of Earth Sciences, University of Western Ontario, 1151 Richmond Street N., London, Ontario, N6A 5B7 Canada

² Institute for Earth and Space Exploration, University of Western Ontario, 1151 Richmond Street N., London, Ontario, N6A 5B7 Canada

³ Lunar and Planetary Laboratory, University of Arizona, 1629 E. University Blvd., Tucson, Arizona, 85721 USA

⁴ Department of Earth, Atmospheric, and Planetary Sciences, Purdue University, 550 Stadium Mall Dr., West Lafayette, IN 47907 USA

⁵ State Key Laboratory in Lunar and Planetary Science, Macau University of Science and Technology, Avenida Wai Long, Taipa, 999078 Macau

Corresponding author: Ethan I. Schaefer (ethan.i.schaefer@gmail.com)

Key Points:

- The fractality of lava flow margins is highly diverse and shows varying scale dependence, even among flows of the same morphologic type.
- Topographic confinement and substrate slopes can modify the fractality of a lava flow's margin without imparting a diagnostic signature.
- We incorporate these complexities in a new framework for interpreting lava flow types from the meter-scale fractality of flow margins.

Abstract

Can fractal analysis of a lava flow's margin enable classification of the lava's morphologic type (e.g., pāhoehoe)? Such classifications would provide insights into the rheology and dynamics of the flow when it was emplaced. The potential to classify lava flows from remotely-sensed data would particularly benefit the analysis of flows that are inaccessible, including flows on other planetary bodies. The technique's current interpretive framework depends on three assumptions: (1) measured margin fractality is scale-invariant; (2) morphologic types can be uniquely distinguished based on measured margin fractality; and (3) modification of margin fractality by topography, including substrate slope and confinement, would be minimal or independently recognizable. We critically evaluate these assumptions at meter scales (1–10 m) using 15 field-collected flow margin intervals from a wide variety of morphologic types in Hawai'i, Iceland, and Idaho. Among the 12 margin intervals that satisfy the current framework's suitability criteria (e.g., geomorphic freshness, shallowly-sloped substrates), we show that 5 exhibit notably scale-dependent fractality and all 5 from lava types other than 'a'ā or pāhoehoe would be classified as one or both of those types at some scales. Additionally, an 'a'ā flow on a 15° slope (Mauna Ulu, Hawai'i) and a spiny pāhoehoe flow confined by a stream bank (Holuhraun, Iceland) exhibit significantly depressed fractalities but lack diagnostic signatures for these modifications. We therefore conclude that all three assumptions of the current framework are invalid at meter scales and propose a new framework to leverage the potential of the underlying fractal technique while acknowledging these complexities.

1 Introduction

Fractal analysis provides an elegant way to describe complex natural geometries such as lava margins (Avnir et al., 1998; Mandelbrot, 1982). It may also hold substantial promise to constrain the rheology, emplacement dynamics, and chemical composition of flows. Bruno et al. (1992) and Gaonac'h et al. (1992) were the first to demonstrate that the geometries of lava flow margins are empirically fractal. That is, the apparent length of these margins, when measured at progressively coarser resolutions, approximately decreases by a power-law over some range of scales. Because fractal geometries naturally arise from nonlinear processes, the fractal analysis of lava margins was expected to provide direct insights into the fluid dynamics of lava flows (e.g., Bruno et al., 1992, 1994; Gaonac'h et al., 1992; Kilburn, 1996). Moreover, Bruno et al. (1992, 1994) and Gaonac'h et al. (1992) presented evidence that the empirical fractality of lava margins might extend from decimeter to kilometer scales, and Bruno et al. (1992, 1994) demonstrated that this fractality could help to discriminate between two morphologic lava types: 'a'ā and pāhoehoe. Knowledge of a flow's morphologic type can, in turn, help to constrain the dynamics, rheology, effusion rate, and crustal disruption history of the lava at the time of its emplacement (e.g., Cashman et al., 1999; Hamilton, 2019; Peterson & Tilling, 1980; Rowland & Walker, 1990). In addition, Bruno et al. (1994) found that flows of intermediate to silicic composition had measured lengths that departed from power-law scaling, at least at scales of hundreds of meters, suggesting that fractal analysis of margin geometries could be used to distinguish mafic lavas from those with more evolved compositions.

Any insights provided by margin fractal analysis would especially facilitate the characterization of flows in remote areas. Although field observations of lava flows provide better constraints (e.g., Harris et al., 2017; Keszthelyi, 2002; Self et al., 1996; Thordarson, 1995), such ground-truthing is not always feasible. For that reason, researchers have used margin fractal

analysis to investigate submarine lava flows on Earth (Maeno et al., 2016; Mitchell et al., 2008; Wroblewski et al., 2019) and flows of lava and impact melt on Mars, Venus, and Earth's moon (Bray et al., 2018; Bruno et al., 1992, 1994; Bruno & Taylor, 1995; Wroblewski et al., 2019; You et al., 1996). As examples, margin fractal analysis may provide constraints on lava type, which in turn could be used to infer eruption style and possibly magma source depths (Wilson & Head, 1994), and supplement radar-derived surface roughness analyses to help clarify the emplacement history of vast volcanic deposits on Venus (Campbell & Campbell, 1992). On Earth, margin fractal analysis may also facilitate the planning of field campaigns. Flow margins could be mapped using remotely-sensed data, and fractal analysis of these margins could reveal distinct populations or anomalous flows that merit further investigation in the field.

The prevailing classification framework for the fractal analysis of mafic lava margins, due to Bruno et al. (1994), depends explicitly on three assumptions: (1) The measured fractality of a margin interval does not critically depend on the scale range over which that fractality is measured. (2) The measured margin fractalities of 'a'ā, pāhoehoe, and so-called transitional lava types are each distinct. (3) The effects of topography, including sloped substrates and confinement, typically render a margin empirically non-fractal rather than merely modulate its empirical fractality. Where this framework is used to classify flows remotely, the results may depend critically on these assumptions. We therefore test each of these assumptions at meter scales (~1–10 m) using 15 field-collected margin intervals from a wide variety of morphologic types in Hawai'i, Iceland, and Idaho (Figure 1).

We first review the relevant background information (section 2) that motivates us to test the assumptions enumerated above. We then explain how we interpret and quantify fractality in this study, including some methodological refinements to the fractal analysis of lava margins (section 3). We present our results (section 4) and then discuss how these results affect the interpretation of morphologic type from margin fractal analysis (section 5), including presentation of a new interpretive framework (section 5.3). Finally, we summarize our principal conclusions (section 6).

2 Background

2.1 Scale dependence

The effective fractal dimension D (section 3.2.2) quantifies the fractality of a geometry. Because D depends on scaling behavior, each measurement of D must be made over a range of scales. Based on this measurement characteristic, a D measured for a natural geometry has traditionally been interpreted to be scale-invariant over the analyzed scale range, that is, to apply consistently across the entire range of scales over which that D was calculated, unless scale dependence is conspicuous. Although mathematical fractals that are self-similar (section 3.2.1) do indeed have scale-invariant fractality, the default assumption of scale-invariant fractality for natural geometries has been questioned by some (e.g., Avnir et al., 1998; Shenker, 1994). (For further discussion, see section 3.2.1.)

In particular, the fractal analysis of topographic contours, including coastlines, provides a cautionary parallel to the fractal analysis of lava margins. The D values of topographic contours were long thought to be scale-invariant (Mandelbrot, 1967; Richardson, 1961), but later work showed that these contours had distinctly different D values when measured over discrete scale ranges (Mark & Aronson, 1984). Still later, Andrieu (1992, 1996b, 1996a) presented evidence

110 that coastlines' D values vary continuously with scale, including D values for the west coast of
111 Britain, which is the archetypal natural fractal (Mandelbrot, 1967; Richardson, 1961).

112 In the divider method (section 3.2.2) used by Bruno et al. (1994) and in the present study,
113 the analyzed scale range for each D is defined by a discrete set of scales. We call such a set a
114 “rod set”, as each scale was traditionally measured using a different physical rod of that length.
115 The parameter r^* provides a single representative length value for a given rod set (section 3.2.4).
116 The lava margin fractal analyses of Bruno et al. (1994) included 27 field analyses, collectively
117 spanning scales of 0.125–16 m, and 17 photographic analyses, collectively spanning scales of
118 12–2400 m. Bruno et al. (1994) did not specify the rod set used in each D measurement, but they
119 did provide some generalities. In each field analysis, they used exactly one rod set (and therefore
120 calculated exactly one D) per margin interval. Moreover, each rod set used in field analysis was
121 selected from a collection of rods with lengths 0.125 m, 0.25 m, 0.5 m, 1 m, 2 m, 4 m, 8 m, and
122 16 m. Wherever possible, they specifically used a rod set of either 1–16 m or 0.5–16 m
123 (corresponding to representative scales of $r^* = 4$ m and $r^* = 2.83$ m, respectively). For shorter
124 margin intervals, they used rods as short as 0.125 m ($r^* \geq 0.5$ m). Their use of only one rod set
125 per field-analyzed margin interval and the preferential use of similar rod sets in field analyses
126 could potentially mask any scale-dependent fractality at meter scales (see also section 5.2.1),
127 which are the focus of the present study.

128

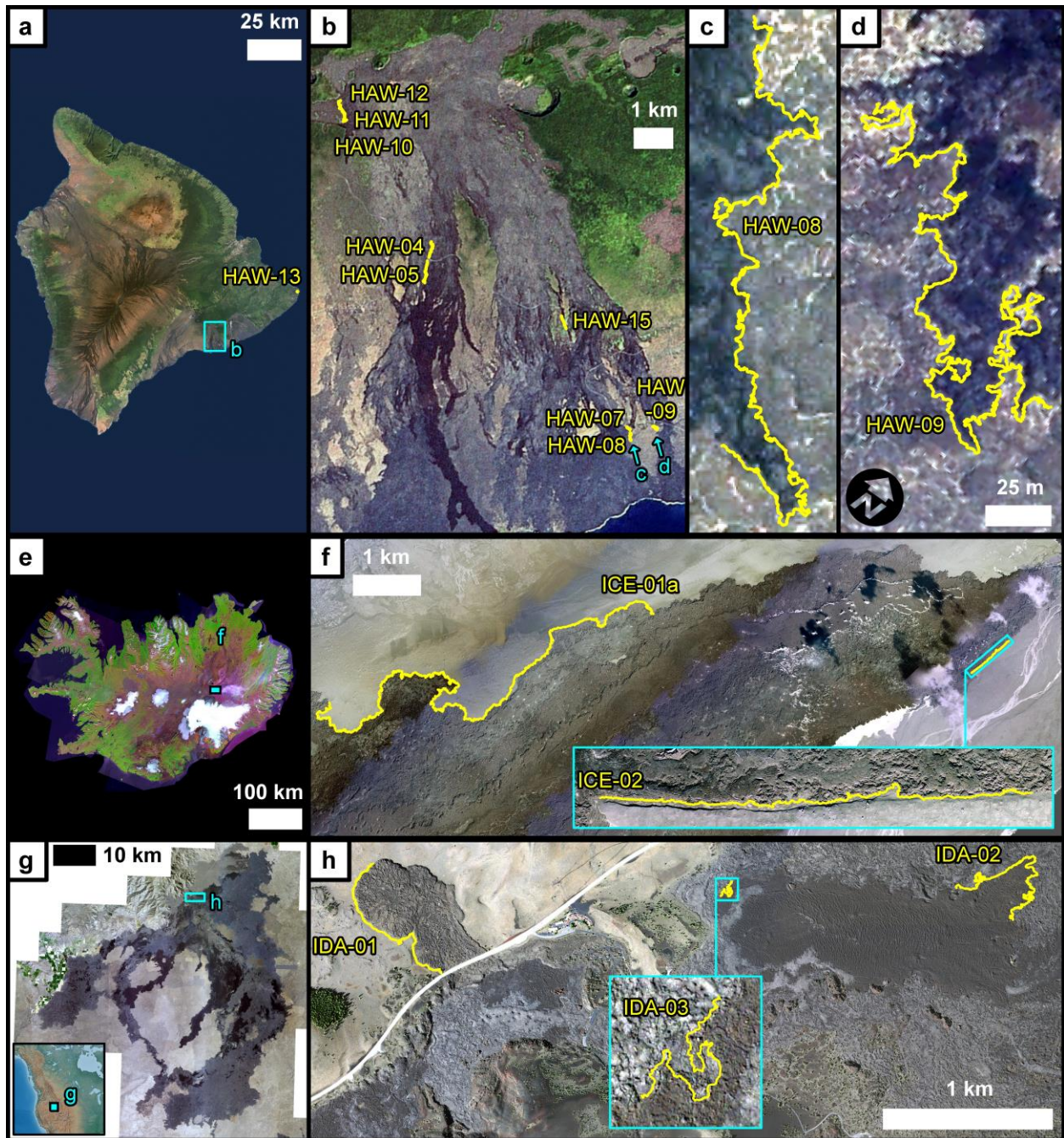


Figure 1. Locations of all 15 margin intervals (yellow lines) analyzed in the present study. (a) The island of Hawai'i. (b) Study area in Hawai'i Volcanoes National Park. (c)–(d): Magnified views of two margin intervals from (b). (e) Iceland. (f) Two margin intervals from the 2014–2015 Holuhraun flow field. (g) Study area and (h) margin intervals in Craters of the Moon National Monument and Preserve, Idaho, USA. Inset in (g) shows location in North America. Background of (a) and (b) is a Landsat 7 mosaic (15 m/pixel) created by Earthstar Geographics. Background of (c) and (d) is a QuickBird orthomosaic (0.6 m/pixel) from the Natural Resources Conservation Service of the United States Department of Agriculture. Background of (e) is a Landsat 8 mosaic (66 m/pixel) created by the National Land Survey of Iceland. Background of

(f) is a color orthoimage from Loftmyndir ehf. (0.5 m/pixel). Backgrounds of (g) and (h) are orthoimages (0.5 m/pixel) from the National Agriculture Imagery Program of the United States Department of Agriculture. North is up in all views except for (d) and the inset in (f).

In three cases, Bruno et al. (1994) also analyzed the same margin—albeit over different intervals—in paired field and photographic analyses. The measured disparities were similar to the single-rod-set along-length variabilities in D that they measured. They therefore interpreted D to be scale-invariant, but the limited scope of these paired analyses—three pāhoehoe margins, all from Hawai‘i, each analyzed with exactly two rod sets (one from the field and one from photographs)—may not be sufficient to characterize the frequency of scale-dependent fractality across morphologic types and geologic settings, especially at meter scales.

When exploring scale dependence, we primarily focus on meter scales (~ 1 – 10 m), though we also report results at coarser scales when possible. Meter scales are best supported by our data and were the primary focus of Bruno et al. (1994), whose study is the most extensive investigation of lava margin fractality to date. The scale dependence of empirical lava margin fractality is also least constrained at these scales, as described earlier in this section. Furthermore, meter scales are relevant in both terrestrial and planetary contexts. These scales are resolvable on Mars by the High Resolution Imaging Science Experiment (HiRISE) on board the *Mars Reconnaissance Orbiter*, which has a minimum pixel scale of 25 cm/pixel (McEwen et al., 2007), and on Earth’s moon by both the Narrow Angle Cameras on board the *Lunar Reconnaissance Orbiter*, which has a minimum pixel scale of 50 cm (Robinson et al., 2010), and the Orbiter High Resolution Camera on board *Chandrayaan-2*, which has a minimum pixel scale of 25 cm (Chowdhury et al., 2020).

2.2 Morphologic lava types

Morphologic lava types are commonly classified in a three-part system of ‘a‘ā, pāhoehoe, and block lava (Harris et al., 2017; Macdonald, 1953). ‘A‘ā and pāhoehoe are most commonly associated with mafic lava, whereas block lavas typically are more silicic (Finch, 1933). Other mafic lavas that are neither ‘a‘ā nor pāhoehoe are conventionally called “transitional” (see section 2.2.2). We direct the reader to Harris et al. (2017), Gregg (2017), and Hamilton (2019) for detailed descriptions of these lava types. Although lava types are traditionally distinguished by sub-meter surface morphology, they can also be identified from interior structure (e.g., Harris et al., 2017; Keszthelyi, 2002; Self et al., 1996; Thordarson, 1995). We include examples of ‘a‘ā, pāhoehoe, and transitional lavas in the present study, as well as one example of lava that may be intermediate between block lava and ‘a‘ā (Table 1).

2.2.1 ‘A‘ā and pāhoehoe

Whether basaltic lava freezes to form a crust of ‘a‘ā or pāhoehoe is determined by both the rheology and dynamics of the flow, with pāhoehoe favored by lower apparent viscosities and lower shear strain rates (Macdonald, 1953; Peterson & Tilling, 1980). These properties can be interpreted as lower yield strengths and lower rates of net crustal disruption, respectively (Cashman et al., 1999; Kilburn, 1990). A flow can also transition from pāhoehoe to ‘a‘ā (or, more rarely, from ‘a‘ā to pāhoehoe) as the apparent viscosity and/or shear strain rate change along the flow’s path (Hon et al., 2003; Lipman & Banks, 1987; Macdonald, 1953; Wolfe et al.,

181 1988). For example, steep substrates can increase local flow velocities and hence shear strain
 182 rate, such that pāhoehoe transitions to ‘a‘ā (e.g., Macdonald, 1953; Peterson & Tilling, 1980).

183 Bruno et al. (1994) primarily focused on margins of ‘a‘ā and pāhoehoe. We therefore
 184 include nine margin intervals of ‘a‘ā or pāhoehoe to facilitate comparison of our results to theirs.

185 2.2.2 Transitional lavas

186 The genetic interpretation of transitional lavas is more complicated than that of ‘a‘ā and
 187 pāhoehoe. Several workers have reported continuous and long-lived formation of transitional
 188 lavas at active flows (e.g., Lipman & Banks, 1987; Pedersen et al., 2017), whereas others have
 189 interpreted transitional lavas to form from episodic disruption of otherwise stable crusts
 190 (Hamilton, 2019; Keszthelyi et al., 2004). Further research is necessary to clarify the origins of
 191 and relationships between transitional types (cf. Cashman et al., 1999; Hon et al., 2003; Kilburn,
 192 1990; Peterson & Tilling, 1980; Soule & Cashman, 2005).

193 To reasonably classify lavas, one must consider transitional types in addition to the
 194 traditional ‘a‘ā and pāhoehoe end-members. For example, pāhoehoe and rubbly lava are the
 195 dominant types in Iceland (Thordarson & Höskuldsson, 2008). Rubbly and slabby lavas may also
 196 be important on Mars, based on the observation of similar morphologies in terrestrial and
 197 Martian flow fields at scales of tens of meters or more (Keszthelyi et al., 2000, 2004; Voigt &
 198 Hamilton, 2018). These observations motivate us to include transitional types in our analysis,
 199 especially as these types have not yet been a major focus of margin fractal analysis (cf. Bruno et
 200 al., 1994). Six of our margin intervals target one or more transitional types, and two of these
 201 intervals come from the outermost margin of the 2014–2015 Holuhraun eruption (Figure 1f),
 202 which was extensively studied while active (e.g., Kolzenburg et al., 2017; Pedersen et al., 2017).
 203 The level, easily traversable sand sheet adjacent to a portion of this margin enabled us to collect
 204 an uninterrupted interval nearly 19 km long (ICE-01a).

205 Note that HAW-13a (Figure S1 of Supporting Information) is unique in the present study
 206 as it is the only margin interval that delineates the boundary between two subtypes within the
 207 same flow. Namely, HAW-13a represents the edge of a subtype of spiny pāhoehoe that Rowland
 208 and Walker (1987) called “primary toothpaste lava.” The surface of this subtype forms a series of
 209 plates and is surrounded by other forms of spiny lava (Rowland & Walker, 1987). Although not
 210 strictly a flow margin, HAW-13a mostly aligns with the margin of the largest primary lobe
 211 mapped by Rowland and Walker (1987) (their Figure 1) and could plausibly be misinterpreted as
 212 a flow margin in remotely-sensed data. This margin interval therefore provides a useful reference
 213 to evaluate the potential for lava flow characterization in the absence of ground truth.

214 2.2.3 Block–‘a‘ā (Highway flow)

215 Finally, we include a margin interval from a lava that may be intermediate between block
 216 lava and ‘a‘ā. This interval (IDA-01) comes from the margin of the informally named
 217 “Highway” flow (Figure 1h) at Craters of the Moon National Monument and Preserve in Idaho,
 218 USA (Hughes et al., 2019; Kuntz et al., 1982; Tolometti et al., 2020).

219 Classic block lavas have thicknesses of tens or even hundreds of meters and are covered
 220 in angular blocks or sub-rounded boulders (Harris et al., 2017). Their surface is generally
 221 vesicle-poor but may have highly vesicular bands (Harris et al., 2017). Highway flow is ~15 m
 222 thick. Its surface includes both rough, viscously-torn slabs, analogous to ‘a‘ā clinker, and

fractured blocks (Hughes et al., 2019; Kuntz et al., 1982; Tolometti et al., 2020). This surface generally has low vesicularity but isolated regions of high vesicularity are exposed on ~1–2% of the surface (Hughes et al., 2019; Sandmeyer et al., 2017).

This flow is among the most evolved of those tested in the area. Chemical analyses typically measure ~62–65 wt% SiO₂ (Kuntz et al., 1985; Leeman et al., 1976; Stout et al., 1994; Tolometti et al., 2020) and qualify the flow as a trachyte or trachydacite (Stout et al., 1994; Tolometti et al., 2020). Although lavas on Mars, for example, generally have more primitive compositions than that of Highway flow, Christensen et al. (2005) measured ~60–63% SiO₂ for one flow using data from the Thermal Emission Imaging System on board Mars Odyssey (Christensen et al., 2004). The alpha proton x-ray spectrometer on the Mars Pathfinder rover also measured rocks in situ with similar SiO₂ content (Economou, 2001; Rieder et al., 1997).

As the single non-mafic margin interval in the present study, the results for IDA-01 cannot be confidently interpreted as general. Nonetheless, these results provide a valuable supplement to the results of other workers at different scales (Bruno et al., 1994; Pyle & Elliott, 2006; Wroblewski et al., 2019).

2.3 Topographic context

There is generally a paucity of meter-scale topographic data available for planetary surfaces, and in high-resolution visual images, shadowing suggestive of the topographic context may be absent if relief is subtle or lighting conditions are ill-suited. Therefore, it may not be possible to independently identify the presence of topographic confinement or significant slopes at meter scales for these locations. Even where sufficiently high-resolution topographic data are available (e.g., Kirk et al., 2008; Moratto et al., 2013; Shean et al., 2016), knowledge of the respective effects of slopes and confinement on empirical margin fractality is essential to interpreting flows in those settings.

Bruno et al. (1994) examined three margin intervals on significant slopes. All three intervals came from 1972 Mauna Ulu ‘a‘ā flows on respective slopes of 11.6°, 14.7°, and 27.8°. Bruno et al. (1994) reported significant modification of empirical fractality only for the margin on the steepest slope and therefore inferred a critical slope angle in the range 15–28°. To further explore the lower end of this range and determine whether any modification of empirical fractality has a scale-dependent component, we include in the present study a 1971 Mauna Ulu ‘a‘ā flow on a slope of ~15° (HAW-15).

The potential for topographic confinement to modify margin fractality has long been recognized (Bruno et al., 1992). However, to our knowledge, no fractal analysis of such a topographically-confined margin has yet been reported. We therefore collected a second Holuhraun margin interval (ICE-02; inset of Figure 1f) that was strongly confined by the right bank of a preexisting stream channel (Bonney et al., 2019). Because both Holuhraun intervals are dominated by spiny pāhoehoe (Voigt et al., 2017), comparison of the confined and relatively unconfined intervals facilitates direct evaluation of the effects of topographic confinement.

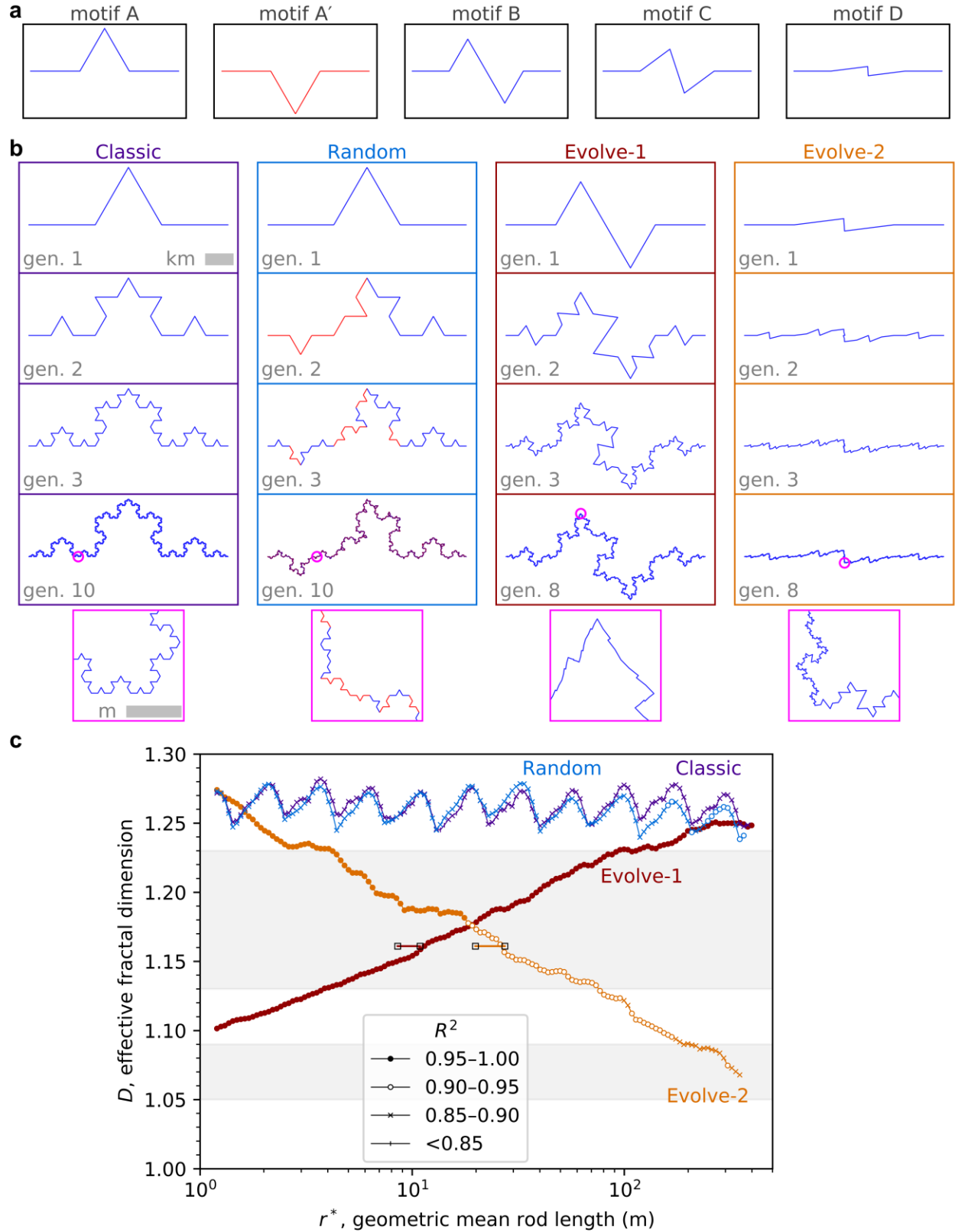


Figure 2. Construction and fractal analysis of some illustrative synthetic geometries. (a) Example motifs used in constructing the geometries. (b) Each geometry is constructed iteratively: generation 1 is a motif from (a), and in each successive generation, every line

segment is replaced by a motif. Classic uses only motif A. For Random, motif A and its flipped counterpart motif A' each have a 50% chance of replacing any segment. Evolve-1 begins with motif B at generation 1, but the motif used at each later generation evolves, by incrementally shortening the middle segment, passing through motif C and culminating with motif D at generation 8. Evolve-2 has the opposite sequence, beginning with motif D and progressing through motif C to motif B at generation 8. Each final geometry has mean segment lengths of 11.8–12.4 cm. All segment lengths are equal for Classic and Random but vary by a factor of 70 for Evolve-1 and Evolve-2 at generation 8. This variation is evident in the magenta-outlined magnified views, which have equal map scale. (c) The results of scale-dependent fractal analysis, or “fractal scale-spectra”, for the final geometries from (b). The theoretical fractal dimension value for both Classic and Random is $D = \frac{\ln(4)}{\ln(3)} \cong 1.26$ (Mandelbrot, 1967), which is reasonably approximated by the analysis. (See also Figure S2 of the Supporting Information.) Motif C is applied at generation 4 for Evolve-1 and at generation 5 for Evolve-2, and has a theoretical $D = \frac{\ln(5)}{\ln(4)} \cong 1.16$ (Mandelbrot, 1967). For Evolve-1 and Evolve-2, a horizontal line at this D value is drawn between the mean and median segment lengths of the corresponding generation. The intersection of these horizontal lines with the Evolve-1 and Evolve-2 scale-spectra suggests that r^* is a reasonable approximation of the scale to which the measured D is sensitive. The pale gray bands are as in Figures 4–6, for reference, and markers indicate R^2 values (section 3.2.2).

3 Methods

3.1 Field measurement techniques

To collect margin interval vertices in the field, we used differential global navigation satellite system (differential GNSS) receivers to collect margin interval vertices. We used two GNSSs: the Global Positioning System (GPS) and the Global Navigation Satellite System (GLONASS).

We walked the length of each margin interval with a differential GNSS rover while a differential GNSS base station simultaneously collected data. In each case, the rover and base station were both Trimble R8s or both Trimble R10s. Depending on the reliability of line-of-sight communication between the rover and base station, we used a sampling interval that was either spatial (e.g., collect one vertex every 10 cm), which requires continuous line-of-sight communication to support a real-time kinematic correction, or temporal (e.g., collect one vertex each second). Table 1 records the resulting variability in inter-vertex spacing.

We postprocessed each vertex using the Trimble Business Center software. The reported horizontal precision is ≤ 3 cm for all vertices. However, we observed the rover mast to slightly tilt at times and estimate our mean measurement error relative to the true margin to be ~ 15 cm (corresponding to a tilt of $\sim 4^\circ$). We provide evidence that this estimate is reasonable in section S1 of Supporting Information. To better simulate the plan-view geometry of orthorectified or nadir-pointing images, all analyses use only the x - and y -coordinates of the postprocessed vertices.

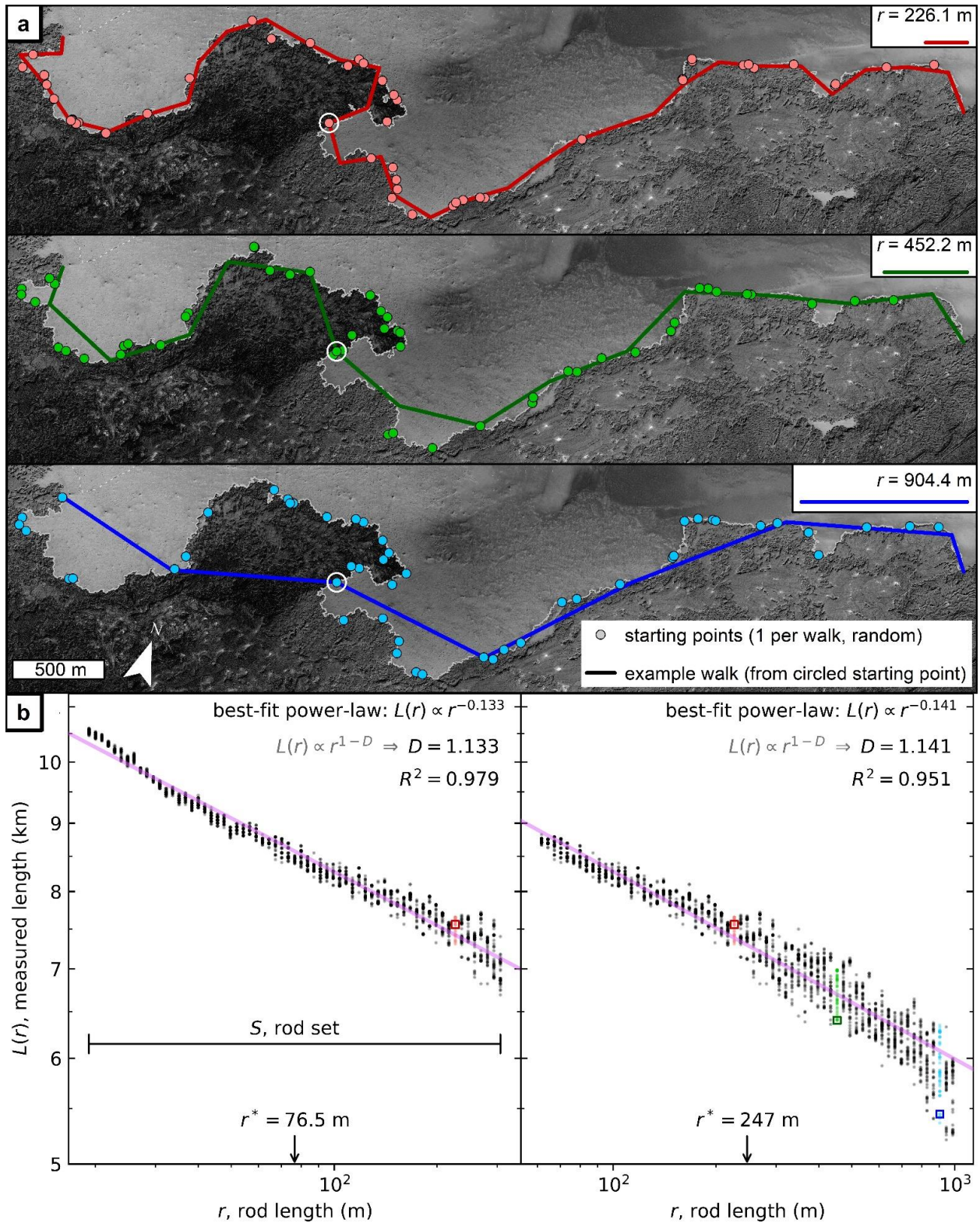


Figure 3. Examples from the fractal analysis of margin interval ICE-01a by the divider method (section 3.2.2). (a) Example data for three different rod lengths. ICE-01a is drawn in light gray. Background is 2015 visible data from Loftmyndir ehf. (0.5 m/pixel). For each rod length, the random starting points for all 50 walked paths are shown as colored dots. Also shown is a single

example path walked with each rod length, starting from the white-circled starting point in each pane. (b) Two log–log Richardson plots. Each shows 50 measured lengths (with each length measured from a different starting point) for each of 65 different rod lengths. The 65 rod lengths in each plot form a rod set. The three selected rod lengths (r values) and their colors correspond in (a) and (b), with the example walks from (a) marked by squares in (b). The representative scale, r^* , is the geometric mean rod length for each rod set (Richardson plot), or equivalently, the median rod length. The effective fractal dimension D is calculated from the trend (which is linear in a log-log plot) of the best-fit power-law (pastel purple), as indicated. The coefficient of determination R^2 measures the goodness of fit and has a maximum of unity (section 3.2.3). The compiled D values from many rod sets analyzing the same margin interval form a fractal scale-spectrum (e.g., Figure 2c). Two Richardson plots are shown to (1) highlight the reuse of results for the same rod length r between different rod sets, such as the results for $r = 226.1$ m (red dots), which appear in both plots, and (2) provide examples of two different R^2 values.

3.2 Fractal analysis

3.2.1 Natural fractality

How the measured fractality of natural geometries should be interpreted has been debated (e.g., Avnir et al., 1998; Shenker, 1994). Early workers (e.g., Mandelbrot, 1967) interpreted such fractality to imply statistical self-similarity. In strictly self-similar geometries, such as the classic Koch curve (Classic in Figure 2), identical geometric patterns are observed when the fractal is viewed across a wide range of scales (Mandelbrot, 1967). For a statistically self-similar geometry, on the other hand, comparable but not identical geometric patterns repeat across a wide range of scales. The random Koch curve (Random in Figure 2) is one such example (Falconer, 2003).

More recently, Mandelbrot (2002) urged greater caution in interpreting natural geometries to be self-similar. Additionally, Gneiting and Schlather (2004) presented a family of synthetic geometries that have formally-defined fractality but are not self-similar, and Li and Li (2017) have since used this family to describe natural phenomena, namely, sea level fluctuations. In this work, we interpret measured fractality to describe the tortuosity of a line rather than imply statistical self-similarity. Likewise, we interpret the effective fractal dimension D as a summary statistic that describes tortuosity over a scale range.

3.2.2 Overview of the divider method

Different fractal analysis methods can yield different effective fractal dimension (D) values (e.g., Gneiting et al., 2012; Klinkenberg & Goodchild, 1992). Moreover, such discrepancies have been specifically reported for lava flow margins (cf. Bruno et al., 1994; Gaonac’h et al., 1992; Luongo et al., 2000). We choose to use the divider method to support comparison to both the large catalog of Bruno et al. (1994) and to most other studies of lava margin fractality (e.g., Blake & Bruno, 2000; Bray et al., 2018; Pyle & Elliott, 2006; Wroblewski et al., 2019).

In the simplest version of the divider method (Figure 3) (Richardson, 1961), a rod of a specified length r_1 is walked along the length of a geometry—for example, a lava margin—such that each end of the rod touches the margin with each step. For each step after the first, the start

of the rod is anchored to the location where the rod ended in the previous step. (Note that the interior of the rod—between its ends—is allowed to intersect the margin.) The apparent length $L(r_1)$ of the geometry, as measured by the rod, is recorded. This same procedure is then repeated with n different rods, each of a different length r_i . If the apparent lengths $L(r_i)$ versus the respective rod lengths r_i used to make those measurements follow a power-law decay, the effective fractal dimension D can be calculated from the best-fit $L(r) \propto r^{1-D}$. Equivalently, these measurements would follow a linear trend with negative slope m on a log–log plot (Figure 3b)—often called a Richardson plot in this context—and the fractal dimension could be calculated from $D = 1 - m$.

When walking a rod along a margin, it is possible that multiple points in the walking direction are exactly a distance r_i from the rod’s start. In this case, our implementation invariably uses the first such point, which Mandelbrot (1986) referred to as a “first exit.” An implementation may instead invariably use the last such point, or “last exit.” The respective D values calculated by first- and last-exit walks are only guaranteed to be equal for self-similar fractals (Mandelbrot, 1986). We adopt the convention to use first exits because Bruno et al. (1992, 1994) adopted this same convention, both in their field and photographic analyses, the latter of which used the EXACT algorithm (Hayward et al., 1989). The first-exit convention is also more computationally efficient (Klinkenberg, 1994).

Following previous workers (e.g., Bruno et al., 1994), we interpret a lava flow margin interval to be empirically fractal if the best-fit $L(r) \propto r^{1-D}$ reasonably describes the trend of the data, as quantified by the coefficient of determination R^2 . Throughout this work, we use “empirical” or “measured” fractality to signal this interpretation of fractality and distinguish it from analytical definitions (cf. Falconer, 2003; Mandelbrot, 1982). Similarly, and following Mandelbrot (1982), we refer to fractal dimensions determined by measurement rather than from theory as effective fractal dimensions but use the variable D for both theoretical and effective fractal dimensions. To calculate R^2 , we use the formula:

$$R^2 = 1 - \sum_{i=1}^n (\hat{y}(r_i) - y_i)^2 / \sum_{i=1}^n (y_i - \bar{y})^2, \quad [\text{Eq. 1}]$$

which supports comparison between linear and nonlinear fits and is one of the formulae recommended by Kvålseth (1985). We perform model fitting using the version of the Levenberg–Marquardt algorithm described by Moré (1978), as implemented in SciPy, a scientific computing package in the Python programming language.

3.2.3 Selection and stepping of rods

To avoid overrepresenting the inter-vertex segments or measurement error in our results, we set the shortest rod used for each margin interval equal to the larger of twice the mean inter-vertex spacing (Andrle, 1992) (Table 1) and twice the estimated measurement error of ~15 cm (section 3.1 and section S1 of Supporting Information). Each successively longer rod has a length $r_i = f r_{i-1}$, where $f > 1$. Such geometric spacing is generally used in fractal analysis (Klinkenberg, 1994) and reflects the scaling of empirical fractals. Following Bruno et al. (1992, 1994), the largest rod used for each margin interval must walk that interval in no fewer than five steps (including the fractional steps described in the next paragraph).

With each rod (Figure 3a), we start walking at a randomly selected point along the margin interval (which is generally not at a vertex) to avoid overrepresenting any particular subset of coordinates (Andrle, 1992). Once the rod has been walked to the end of the margin

interval, we restart walking from the randomly-selected point in the opposite direction and sum the lengths measured in each direction (Andrle, 1992). When the final step of a walk would overshoot the end of a margin interval (as is generally the case), the residual straight-line distance to the end vertex is added to the measured length. This addend is intended to mitigate systematic error (Andrle, 1992; Klinkenberg, 1994). The entire procedure is then repeated 49 more times with each rod, each time from a newly selected random point, following Andrle (1992).

3.2.4 Rod sets and rod set sequences

The scale dependence of the effective fractal dimension D is a major focus of the present study but has not been emphasized in previous studies of lava margins (section 2.1) or other geomorphic features (Andrle, 1996b, 1996a). D must be calculated over a range of scales. Therefore, to describe the scale dependence of D , we must calculate D over many scale ranges for each margin interval. Each such scale range is defined by the range of rod lengths used in the analysis. We refer to the sequence S of rod lengths r that span such a scale range as the “rod set” for that analysis (Figure 3b). Thus, for each analysis k , which yields a single D value, $S_k = (r_{i=1}, r_{i=2} \dots r_{i=n})|_k$. For simplicity of reference, and following Andrle (1992), we will treat the geometric mean of a rod set $r^* = (\prod_{i=1}^n r_i)^{1/n}$ as the representative scale of that rod set. Because each rod set in the present study is composed of an odd number ($n = 65$) of logarithmically-spaced rod lengths, r^* is also the median rod length of each rod set. Although r^* is a non-rigorous convenience, it provides a plausible reference value (Figure 2c).

To define a rod set, any two of three interdependent parameters must be specified: the inter-rod factor $f = r_{i+1}/r_i$, the number of rods n in the rod set, and the factor-range of the rod set $F = r_n/r_1$. Andrle (1992) observed that a larger n reduced random scatter in the calculated D values but also noted that a larger F would yield a poorer model fit in the presence of any systematic divergence from a power-law trend (e.g., curvature on a Richardson plot; Figure 3b). On that basis, he suggested the use of a large n and a small F . However, we interpret D as a summary statistic that describes tortuosity over a scale range, roughly analogous to a moving average of scale-dependent tortuosity (where the averaging window moves along the r^* axis). In that interpretation, F should be sufficiently large to avoid variability due to random noise but not larger than that, to preserve as much scale resolution as possible and support as many rod sets as possible for a given geometry.

Guided by these goals, we use $F = 16$ and $n = 65$, implying $f = F^{1/(n-1)} = 16^{1/64} \cong 1.044$, throughout the present study. These parameters satisfy the recommendation $n \geq 5$ of Klinkenberg (1994) and facilitate comparison to the field analysis results of Bruno et al. (1994), who preferred $F = 16$ or 32, $n = 5$ or 6, and $f = 2$ for margin intervals as long as those in the present study (section 2.1). Each D value is therefore calculated by fitting 3250 apparent lengths (Figure 3b), which come from 50 iterations with each of 65 rod lengths in a rod set. The D value for each rod set is plotted against r^* on a log–log plot. We call the entire sequence of scale-dependent D values plotted for a given margin interval a “fractal scale-spectrum” (cf. Figure 7 of Andrle (1992) and Figure 4 of Maria and Carey (2002)). For example, the fractal scale-spectra in Figure 2c reflect how the tortuosity of Evolve-1 and Evolve-2 vary with scale.

The ratio between the corresponding scales (e.g., minimum, maximum, representative) of consecutive rod sets is the inter-rod-set factor $I = (r_i|_{k+1})/(r_i|_k)$. We invariably set $I = f$

throughout this study. This correspondence permits rod-stepping results to be reused between overlapping rod sets, because $r_i|_k = r_{i-1}|_{k+1}$ (e.g., red dots in both plots of Figure 3b). This reuse facilitates an extreme savings in computation time. Unfortunately, this reuse also reduces the independence of D values calculated with overlapping rod sets. Nonetheless, the use of 50 iterations (starting points) sufficiently reduces variability in calculated D values (Andrle, 1992) that the reuse of rod-stepping results has no significant effect on our general results.

3.2.5 Comparison to the Hurst exponent

For reference, we note another measure, called the Hurst exponent. The Hurst exponent has been used to characterize rough geologic surfaces in both terrestrial and planetary contexts (Neish et al., 2017; Shepard et al., 1995, 2001). Though fractality is often discussed when applying the Hurst exponent, the measure is generally independent of fractality (Gneiting & Schlather, 2004). Nonetheless, in the special case of self-similar geometries (section 3.2.1), the Hurst exponent H is simply related to D by $D = H - 3$ for surfaces and $D = H - 2$ for profiles (e.g., Shepard et al., 1995).

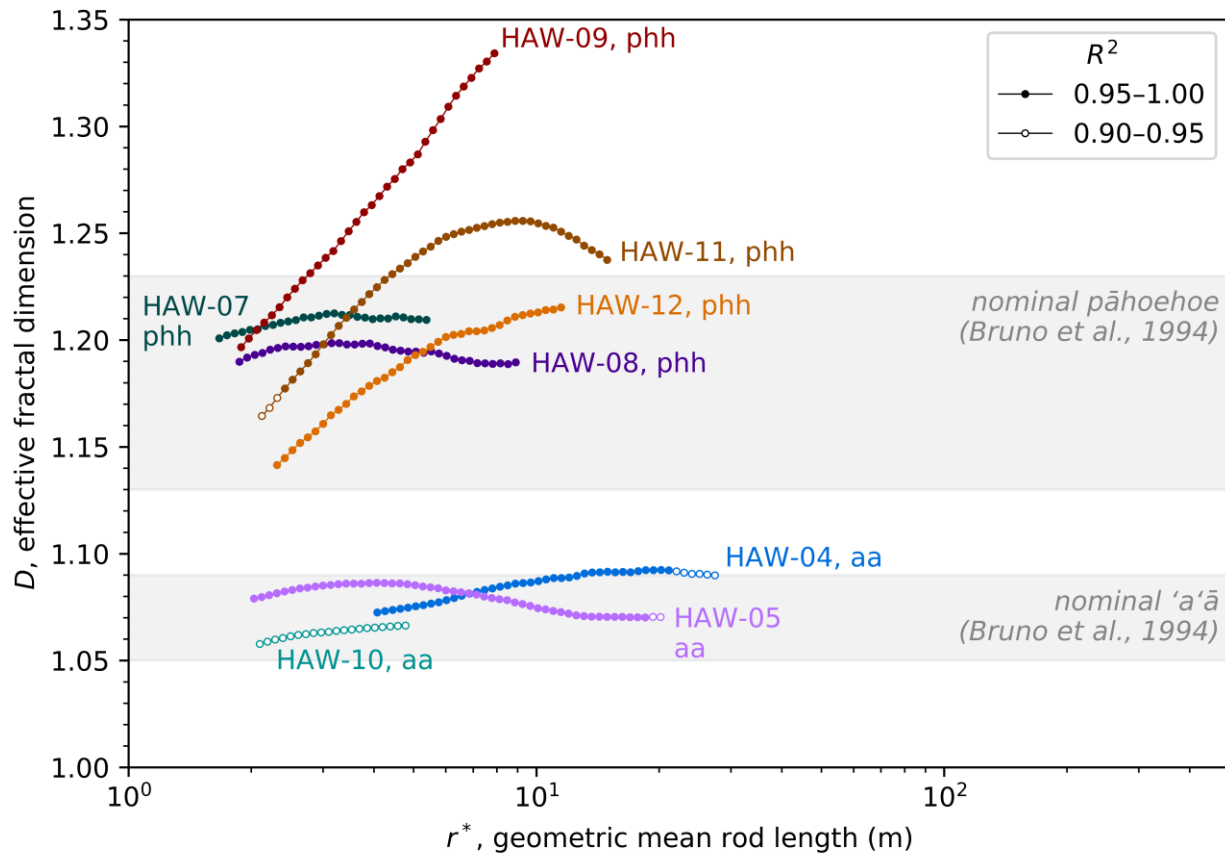


Figure 4. Fractal scale-spectra for ‘a’ā (HAW-04, -05, and -10) and pāhoehoe (HAW-07, -08, -09, -11, and 12) margin intervals compared to nominal ranges (shaded gray) for ‘a’ā and pāhoehoe from Bruno et al. (1994). None of these margin intervals have acute topographic effects. See Table 1 for explanation of morphologic codes (e.g., phh).

4 Results

The fractal analysis results for ‘a‘ā and pāhoehoe margin intervals on shallow slopes (generally $\lesssim 4^\circ$), that lack substantial topographic confinement, are presented in Figure 4. The results for other morphologic types that likewise are not subject to acute topographic effects are presented in Figure 5. Finally, the results for an ‘a‘ā margin interval on a 15° slope (HAW-15) and a spiny pāhoehoe margin interval confined by a stream channel (ICE-02) are presented in Figure 6. In these plots, scale-invariant behavior is indicated by a constant fractal dimension D as the geometric mean rod length r^* changes, and hence, a horizontal trend. Conversely, scale-dependent behavior is indicated by variation in D as r^* changes.

4.1 Scale dependence

In general, the examined margin intervals exhibit a wide range of scale-dependent to relatively scale-independent empirical fractal behavior. For discussion purposes, we will adopt the criteria of Bruno et al. (1994) in this section to identify scale-dependent empirical fractality. Bruno et al. (1994) discarded all fractal analyses for which $R^2 \leq 0.95$ or for which slope or topographic confinement are significant. Twelve margin intervals satisfy these criteria. Bruno et al. (1994) further interpreted empirical fractality to be scale-independent if the observed variation in D was $\lesssim 0.05$. Based on that criterion, 7 of the remaining 12 margin intervals (HAW-04, HAW-05, HAW-07, HAW-08, HAW-13a, IDA-01, and IDA-03) have scale-independent empirical fractality, with observed D variation of 0.01–0.05, and 5 (HAW-09, HAW-11, HAW-12, ICE-01a, and IDA-02) have scale-dependent empirical fractality, with observed D variation of 0.07–0.17. For reference, note that relaxing the minimum required R^2 to 0.90 (Anderson et al., 2005; You et al., 1996) would cause 13 margin intervals to be included: HAW-10 would be added to the list of scale-independent margin intervals (Figure 4) and IDA-03 and HAW-13a would switch from scale-independent to scale-dependent, with D variations of 0.08 and 0.06, respectively (Figure 5).

Returning to the $R^2 > 0.95$ criterion, all five of the margin intervals with scale-dependent empirical fractality have a maximum effective fractal dimension $D_{\max} \gtrsim 1.19$. The fact that margin intervals with lower D_{\max} values do not exhibit greater variation in D may partially reflect their proximity to the lowest possible value $D = 1$. However, one cannot generalize that margin intervals with low D values have little variation in D and margin intervals with high D values have large variation in D . For example, D values measured for IDA-02 range from the relatively low $D_{\min} \approx 1.08$ at $r^* \approx 1.20$ m to the relatively high $D_{\max} \approx 1.25$ at $r^* \approx 35.2$ m, a span of ~ 0.17 . For comparison, 24 of the 27 margin intervals measured by Bruno et al. (1994) in the field fall in the same range of D values, 1.08–1.25, measured for IDA-02 alone, including all pāhoehoe and transitional margin intervals and most (4 of 7) ‘a‘ā margin intervals. At the other extreme of variability, two pāhoehoe intervals from the same margin on Mauna Ulu, HAW-07 and HAW-08, each have D values that vary by ~ 0.01 across the analyzed scales (r^* of 1.67–5.37 m and r^* of 1.87–8.90 m, respectively), despite having $D_{\min} \gtrsim 1.20$.

4.2 Topographic effects

Two margin intervals are subject to acute topographic effects and therefore violate what Bruno et al. (1994) called their “simple-case” criteria (Figure 6). To enable some useful comparisons, we will only exclude in the present section those results for which $R^2 \leq 0.90$, similar to You et al. (1996) and Anderson et al. (2005). Nonetheless, the general behavior

described here is at least suggested by those results that meet the more restrictive $R^2 > 0.95$ criterion (cf. section 4.1).

Compared to the other three ‘a‘ā margin intervals, HAW-15, on a slope of 15° , has much lower D values. Its D_{\max} is 1.05, measured at $r^* = 1.20$ m. No other margin interval in this study, except for the topographically-confined ICE-02, has a D value as low at any analyzed scale, and the lowest D value measured by Bruno et al. (1994) on a slope $\leq 15^\circ$ was likewise 1.05. HAW-15’s D_{\min} is 1.02, measured at $r^* = 16.9$ m, which is the lowest D measured in the present study. The lowest D reported by Bruno et al. (1994) was also 1.02 and was measured for another Mauna Ulu ‘a‘ā margin interval on a 28° slope.

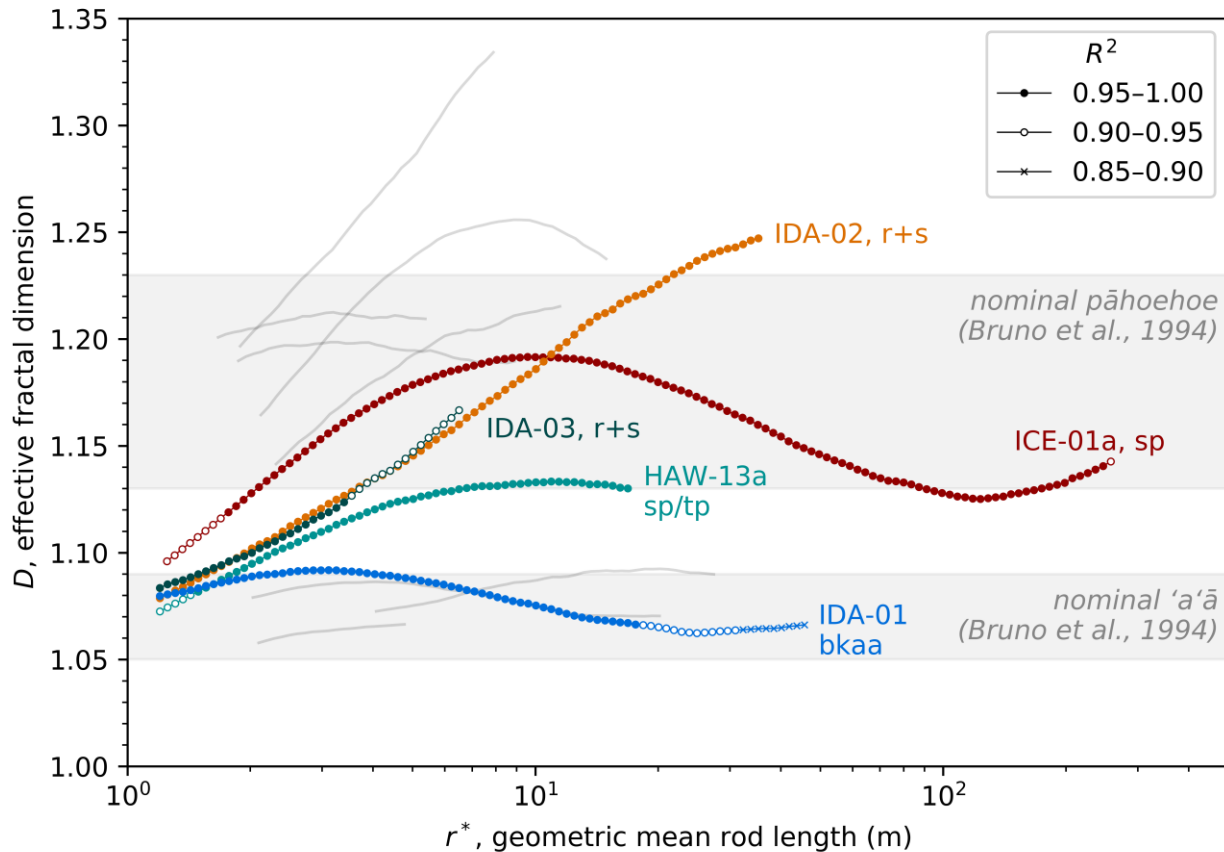


Figure 5. Fractal scale-spectra for spiny pāhoehoe (ICE-01a), block-‘a‘ā (IDA-01), rubbly and slabby lava (IDA-02 and IDA-03), and primary toothpaste (HAW-13a) margin intervals, with fractal scale-spectra from Figure 4 shown as unmarked gray lines, for comparison. None of these margin intervals have acute topographic effects. See Table 1 for explanation of morphologic codes (e.g., r+s).

D values for the Holuhraun margin interval confined by a stream channel, ICE-02, are likewise much lower than D values measured at the same scales for the relatively unconfined Holuhraun margin interval, ICE-01a. Over r^* of 1.25–19.1 m, and requiring $R^2 > 0.90$, D values measured at equivalent scales are 0.037–0.146 less for ICE-02 than for ICE-01a. The respective

ranges of D values over those scales are also disjoint: D of 1.04–1.07 for ICE-02 but D of 1.10–1.19 for ICE-01a.

5 Discussion

5.1 Consequences for interpretation

5.1.1 Intrinsic variability of basaltic lava margins

Our analyses of ‘a‘ā and pāhoehoe margin intervals (Figure 4) reproduce the general results of comparable analyses by Bruno et al. (1994). Namely, these results are that ‘a‘ā and pāhoehoe margins have distinct typical D ranges that do not overlap, with the D values of pāhoehoe margins systematically higher than those of ‘a‘ā margins. Our results also largely reproduce the quantitative details of those of Bruno et al (1994). Their field analyses correspond to r^* of 0.5–4 m, with a preference for $r^* = 4$ m and $r^* = 2.83$ m (section 2.1). At $r^* < 4$ m, the results for our three ‘a‘ā intervals (after rounding to the nearest hundredth) all fall within the nominal ‘a‘ā range of 1.05–1.09 that Bruno et al. (1994) identify, though they would have rejected the results for HAW-10 for having $R^2 \leq 0.95$. Similarly, at these scales, only the results for HAW-09 of the five pāhoehoe intervals is outside the nominal pāhoehoe range of 1.13–1.23, at $r^* > 2.7$ m.

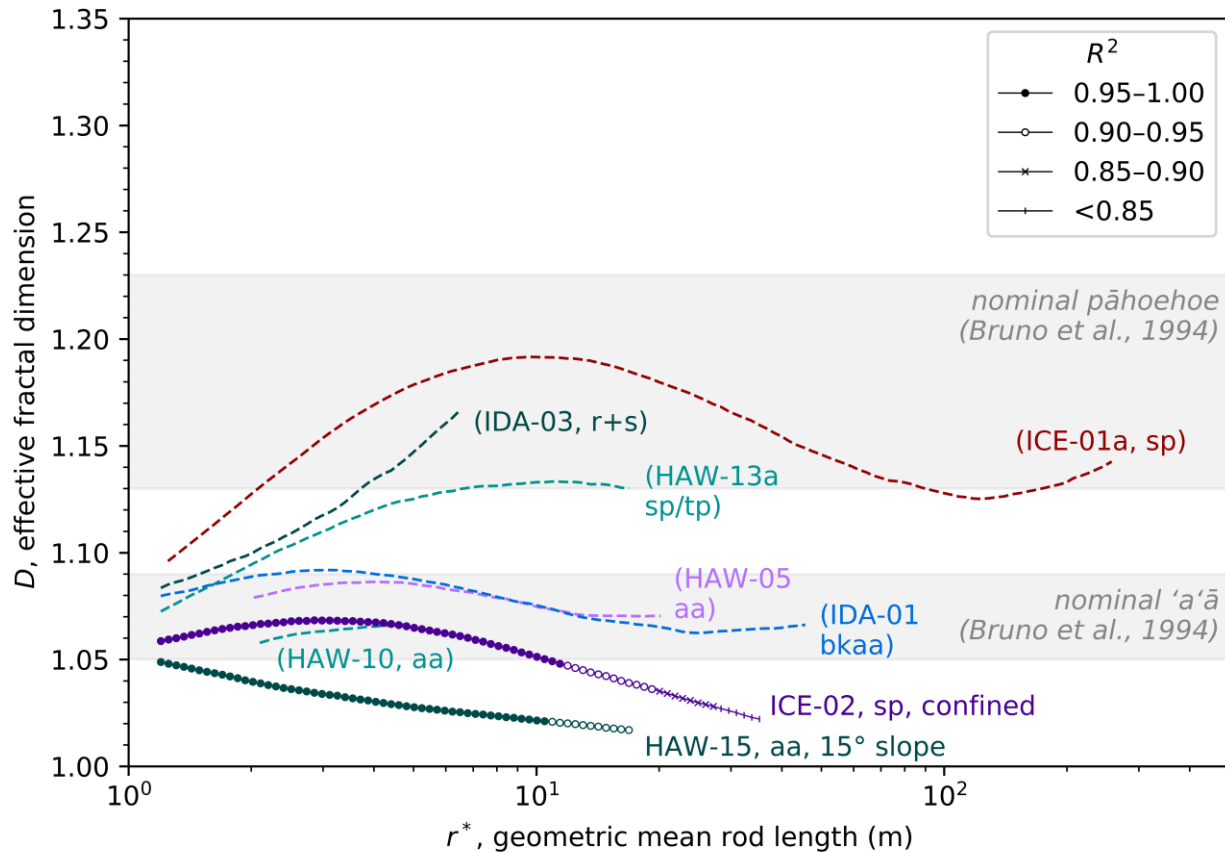


Figure 6. Fractal scale-spectra for ‘a‘ā margin interval on 15° slope (HAW-15) and spiny pāhoehoe margin interval that was confined by a preexisting stream channel (ICE-02).

Additional fractal scale-spectra from Figures 4 and 5 for select margin intervals are shown as dashed lines with parenthetical labels and no markers, for comparison: spiny pāhoehoe ICE-01a, rubbly and slabby lava IDA-03, primary toothpaste HAW-13a, ‘a‘ā HAW-05, ‘a‘ā HAW-10, and block-‘a‘ā IDA-01. These additional margin intervals are on shallow slopes $\lesssim 4^\circ$ and relatively unconfined. See Table 1 for explanation of morphologic codes (e.g., r+s).

However, our results for other morphologic types significantly complicate this picture (Figure 5). Even if we consider only basaltic margins and exclude results for which $R^2 \leq 0.95$, every analyzed margin interval for a morphologic type other than ‘a‘ā and pāhoehoe has at least some D values in the nominal ‘a‘ā and/or pāhoehoe ranges of Bruno et al. (1994). Measured D values fall in the nominal pāhoehoe range for spiny pāhoehoe ICE-01a at r^* of 2.01–247 m (rounding D to the nearest hundredth), for rubbly and slabby lava IDA-02 at 3.07–21.9 m, and for primary toothpaste HAW-13a at 6.79–16.9 m. Similarly, D values fall in the nominal ‘a‘ā range for rubbly and slabby lava IDA-02 at r^* of 1.20–1.56 m, rubbly and slabby lava IDA-03 at 1.20–1.49 m, and primary toothpaste HAW-13a at 1.49–1.78 m.

Taken together, the widely varying scale dependence of empirical margin fractality among the analyzed intervals and the frequently overlapping D ranges of the analyzed morphologic types indicate that D , when measured with a single rod set, is not a reliable, independent indicator of morphologic type at meter scales (that is, for r^* of ~ 1 –10 m). It further seems unlikely that the shape of the fractal scale-spectrum has the potential to serve as a discriminator of morphologic type at meter scales. For example, among pāhoehoe margin intervals, the fractal scale-spectra (Figure 4) for HAW-07 and HAW-08 (Figure 1c) are distinctly different from those of HAW-09 (Figure 1d), HAW-11, and HAW-12.

Moreover, primary toothpaste HAW-13a, which is the only interval along an internal subtype margin (section 2.2.2), does not have a distinguishing scale-spectrum. Although primary toothpaste is a subtype of spiny pāhoehoe, its scale-spectrum nearly coincides with that of rubbly and slabby lava IDA-03 over r^* of 1.49–3.39 m (excluding results with $R^2 \leq 0.95$) (Figure 5). The curvature of the HAW-13a scale-spectrum is also similar to that of the spiny pāhoehoe ICE-01a scale-spectrum, and the results for HAW-13a have high R^2 values (>0.90 and typically >0.95) similar to those for flow margin intervals. These observations suggest that subtype margins within flows may not be readily distinguished from flow margins by their fractality (cf. Anderson et al., 2005).

5.1.2 Margins of non-mafic composition

For block-‘a‘ā IDA-01, which has intermediate composition, we measure D values of 1.07–1.09 for r^* of 1.2–17.6 m (which use r of 0.3–70.4 m). This result is in reasonable agreement with those of Bruno et al. (1994), who measured D values of 1.08–1.17 for $r < 31.6$ m and 1.09–1.20 for r of 31.6–100 m among five margin intervals of basaltic andesite. (Bruno et al. (1994) do not specify the rods used and therefore r^* cannot be calculated.) At coarser scales, Bruno et al. (1994) measured systematically higher D values. For example, they reported D values of 1.20–1.46 for four of these margin intervals at r of 316–1995 m. They therefore concluded that margin intervals of intermediate composition, unlike those of mafic composition (cf. section 4.1), have scale-dependent fractality. Moreover, they speculated that lower D values

at fine scales may be due to the suppression of nonlinear flow dynamics at these scales, resulting in non-fractality.

However, we note that the fractal scale-spectra for IDA-01, which has intermediate composition, and HAW-05, which has basaltic composition, nearly coincide across their overlapping scales, r^* of 2.03–20.3 m (requiring $R^2 > 0.90$) (Figure 6). This correspondence suggests that margin intervals of intermediate composition are not necessarily less fractal than those of basaltic composition and that fractal analysis may not be able to distinguish between ‘a‘ā margin intervals, like HAW-05, and block–‘a‘ā margin intervals, like IDA-01. Similarly, Pyle and Elliott (2006) concluded that fractal analysis with a single rod set cannot discriminate between basaltic ‘a‘ā margins and dacitic block–‘a‘ā margins based on analysis of 10 dacitic block–‘a‘ā margin intervals from the Kameni Islands, Greece at $r^* = 10$ m (r of 1–100 m). In addition, Wroblewski et al. (2019) calculated single- r^* D values of 1.03–1.11 at r^* of 152–802 m for five subaerial margin intervals of intermediate to felsic composition. It is not currently clear how these relatively low D values relate to the higher D values measured by Bruno et al. (1994) at similar (coarse) scales and for similar compositions.

5.1.3 Topographic context

Interpretation of morphologic type from margin fractal analysis is further complicated by topographic context (Figure 6). The margin interval from a Mauna Ulu ‘a‘ā flow on a 15° slope, HAW-15, generally has very low D values. These D values are lower than those of any other margin interval in the present study and lower than any result of Bruno et al. (1994) for a margin interval on a shallower slope. These observations strongly suggest that HAW-15’s D values are depressed relative to the intrinsic D of an ‘a‘ā margin interval. That is, these are lower than the D values that would be expected for a similar flow margin interval on a shallow slope without topographic confinement.

Similarly, Bruno et al. (1994) measured their lowest D value, 1.02, for another Mauna Ulu ‘a‘ā margin interval on a 28° slope. Based on that observation, they likewise inferred that steep slopes could depress D values. However, they also calculated an unusually low $R^2 = 0.78$ for that interval. This result led them to conclude that empirical “fractal behavior... break[s] down, with an accompanying decrease in D , on steep (>15–28°) slopes.” Conversely, the results for HAW-15 have $R^2 > 0.95$ across most analyzed scales (namely, for r^* of 1.20–10.5 m). These high R^2 values indicate that a margin’s D can be significantly depressed by steep slopes without an associated loss of empirical fractality. Interestingly, Bruno et al. (1994) measured their two lowest D values at field scales for two Mauna Ulu ‘a‘ā margin intervals on slopes of 11.6° and 14.7°, with $R^2 = 0.99$ for both results. These observations could likewise suggest depressed D values combined with retention of empirical fractality, though the intrinsically low D values of ‘a‘ā margins complicates that interpretation.

Comparison of the results for spiny pāhoehoe ICE-02, which is confined by a channel, to those of its relatively unconfined counterpart, ICE-01a, strongly suggests that the D values of ICE-02 are also depressed. In addition, the results for ICE-02, like those for HAW-15, have $R^2 > 0.95$ across meter scales (namely, for r^* of 1.20–11.4 m). However, the topographic relief is distinctly different in each case. For HAW-15, flow is down dip and the 448 m margin interval falls 88 m vertically along its length. For ICE-02, flow is along strike and parallel to a bank ~10 m high (Bonnefoy et al., 2019, including their Figure 10). Moreover, when we observed the

margin in August 2015, the surface relief along portions of the interval was as low as ~2 m due to post-eruption fluvial modification (Bonnefoy et al., 2019, including their Figure 12).

The results for both HAW-15 and ICE-02 indicate that margin D values can be significantly depressed at meter scales by local topography without destroying empirical fractality. Therefore, low R^2 values for margin fractal analyses cannot be relied upon to recognize and exclude results modified by topography. In the absence of independent knowledge of local topography, a margin with low measured D may indicate a morphologic type with intrinsically low D , such as ‘a‘ā, or a morphologic type with intrinsically high D , such as pāhoehoe, that was topographically confined or emplaced on a slope. Moreover, even where topographic data are available, one must consider the potential that terrain adjacent to a lava margin was modified post-emplacement, as occurred along the ICE-02 interval. In the case of such modification, the extant surface relief could be below the vertical resolution of the data even if the original constraining height had been much greater.

5.2 Our results in context

5.2.1 Scale dependence

Our study focuses primarily on meter scales, that is, r^* of ~1–10 m. Only 6 of our 15 fractal scale-spectra extend to scales of $r^* > 20$ m, and only the results for ICE-01a extend to $r^* \geq 100$ m.

Across meter scales, we observe significant variation in measured D values for 5 of the 12 margin intervals that meet the selection criteria of Bruno et al. (1994) (section 4.1). (Of the 15 margin intervals that we analyzed, Bruno et al. (1994) would have excluded HAW-15 and ICE-02, which are acutely affected by topography, and HAW-10, for which no measurement attained $R^2 > 0.95$.) At first glance, these results would appear to conflict with those of Bruno et al. (1994). Bruno et al. (1994) report no systematic differences in D between their 27 field analyses, which used r of 0.125–16 m and preferred $r^* = 4$ m and $r^* = 2.83$ m, and their 17 photographic analyses, which used r of 12–2400 m. For three margins, but different intervals, they also directly compared the D values measured in the field to those measured from photographs at coarser scales and found differences similar to along-length variations in D measured at a single r^* .

We propose that our results and those of Bruno et al. (1994) can be reconciled by considering measurement scale and methodology. Only the field analyses of Bruno et al. (1994) correspond to the meter-scale focus of our study. In those field analyses, Bruno et al. (1994) measured each margin interval with only a single rod set, and therefore, at a single r^* . These measurements are thus equivalent to sampling a single point from each fractal scale-spectrum (e.g., Figure 4). If these fractal scale-spectra vary as widely as those that we report, the scatter of the sampled D values would appear random. Consequently, the variability in measured D that Bruno et al. (1994) report between margin intervals may include scale-dependent variability as well.

5.2.2 Physical interpretation

Bruno et al. (1992, 1994) and Gaonac’h et al. (1992) interpreted basaltic flow margins to have scale-independent empirical fractality across decimeter to kilometer scales (see section

5.2.1). This interpretation led both them, and others (Anderson et al., 2005; Blake & Bruno, 2000; Kilburn, 1996), to either speculate on the physical implications of the inferred statistical self-similarity or search for specific physical origins. However, even scale-independent empirical fractality does not imply statistical self-similarity (section 3.2.1). Moreover, we measure scale-dependent fractality for 5 of 12 suitable margin intervals at meter scales (section 4.1), and for ICE-01a and IDA-02 at decameter scales. This scale dependence, as well as the broad range of scale-dependent to relatively scale-independent behaviors that we observe, suggests that physical insights based on the putative self-similarity of lava margins should be viewed with caution. More generally, although fractal analysis facilitates quantitative descriptions of natural geometries, it should not be interpreted to provide insight into the underlying physics unless such an inference is independently supported by theory (e.g., Avnir et al., 1998; Neuman et al., 2013).

5.3 New interpretive framework

In section 5.1, we primarily highlighted the ways in which our results are not consistent with the interpretive framework of Bruno et al. (1994). Nonetheless, there are also ways in which our results correspond, at least approximately, to those on which Bruno et al. (1994) developed their interpretive framework (e.g., the first paragraph of section 5.1.1). These points of correspondence suggest that the underlying technique—namely, the fractal analysis of lava margins—retains some of the same interpretive potential originally recognized by Bruno et al. (1994). To realize this potential, we propose a modified framework that is informed by the new insights, constraints, and sources of uncertainty identified by both the present study and other recent research.

5.3.1 Flow suitability and recommended methods

Our framework draws primarily from two studies: the present one and that of Bruno et al. (1994). Therefore, the best-suited flows are those that are compatible with the selection criteria used in these studies, and the framework requires the use of similar methods.

The flows analyzed by Bruno et al. (1994) and in the present study (Table 1) are from Earth, were emplaced subaerially, and are geologically young. These criteria imply a host of conditions that can affect eruptions and flow emplacement but differ between planetary bodies, such as gravitational acceleration, and/or with geologic time, such as atmospheric density, ambient temperature, lava composition, and effusion rate (e.g., Self et al., 1998; Wilson & Head, 1994). We could conceivably expand the range of conditions sampled if we included submarine lava flows from Earth, but the margin fractality of these flows has not been extensively studied and existing results are ambiguous (Maeno et al., 2016; Mitchell et al., 2008; Wroblewski et al., 2019). We therefore consider only young, subaerial terrestrial lava flows to be best suited to the framework. Nonetheless, the utility of this framework to such lava flows suggests that margin fractal analysis likely has value for studying lava flows in other environments and may facilitate the identification of terrestrial analogs for flows on other planetary bodies. For example, margin fractal analysis could complement studies of planetary lava flows that have focused on morphology, radar-derived surface roughness, and topographic roughness to relate those flows to examples from Earth (Bruno & Taylor, 1995; Campbell & Campbell, 1992; Hamilton et al., 2020; Keszthelyi et al., 2004; Tolometti et al., 2020; Whelley et al., 2017).

Best-suited flows are also geomorphically fresh and lack significant topographic confinement. Any modification or obscuration of the margin by weathering, erosion, or mantling

would likely also modify the margin's meter-scale fractality. In the present study, the topographic confinement of ICE-02 significantly depressed its margin D (section 5.1.3). However, more generally, it is plausible that topographic confinement may either increase or decrease margin D depending on the fractality of the confining topography. For example, consider the extreme case in which the confining topography is very steep. In that case, the confining walls would effectively form a mold that is filled by the flow. This interpretation that the modification of margin D by confining topography depends on the geometry of that confining topography is consistent with our results for ICE-02. The stream channel that confines ICE-02 is smooth and straight relative to the tortuous geometry of the relatively unconfined ICE-01a, and that confinement depresses the margin D of ICE-02.

Measured fractal dimension values are sensitive to the method used and even to details of its implementation (section 3.2.2). Therefore, those who wish to use this framework are encouraged to use the same code as the present study (Schaefer, 2020b). Moreover, we only propose this framework for use at meter scales. The results of the present study explicitly consider scale, and the field-based results of Bruno et al. (1994) focus on a narrow range of scales. These combined results therefore describe 42 margin intervals at meter scales with sufficient detail so that scale dependence can be reasonably assessed. Conversely, the photographic analyses of Bruno et al. (1994) are scattered across a wide range of coarser scales, and with few exceptions, the relevant scales for each result are not reported. The results of the present study are also not well suited to explore those coarser scales (see section 5.2.1).

5.3.2 High margin D

For basaltic flows, Bruno et al. (1994) interpreted margin $D > 1.13$ to suggest pāhoehoe. We interpret margin $D \geq 1.13$ to be consistent with pāhoehoe at meter scales for best-suited flows but not uniquely indicative of that type, as transitional lava types may also have high margin D values at these scales (section 5.1.1). However, if a margin $D \geq 1.20$ is measured for a best-suited lava flow margin at meter scales, pāhoehoe is suggested, based on reported observations to date. All four of the pāhoehoe margin intervals in our study attain $D \geq 1.20$ (rounded to the nearest hundredth) within r^* of 1–10 m, and no margin interval of another morphologic type attains such a high D value over these scales in the present study. Similarly, the only 4 basaltic margins that attain $D \geq 1.20$ at meter scales in the catalog of Bruno et al. (1994) are all pāhoehoe, though 11 more pāhoehoe margins have $D < 1.20$. Although Bruno et al. (1994) did not analyze non-mafic lava margin intervals at meter scales, they reported decreasing margin D values at finer scales for such intervals down to $r = 10$ m and measured $D \geq 1.20$ only at scales of $r \geq 31.6$ m. Wroblewski et al. (2019) also measured $D \sim 1.28$ at $r^* = 152$ m for a dacite lobe that entered the ocean, though Pyle & Elliott (2006) measured $D = 1.05$ for $r^* = 10$ m for another lobe from the same eruption that was emplaced subaerially. For the non-mafic IDA-01 in the present study, we measure $D \leq 1.09$ (rounded to the nearest hundredth) across meter scales.

However, the margin of rubbly and slabby IDA-02 has $D \geq 1.20$ for $r^* \geq 11.4$ m, and no meter-scale result of Bruno et al. (1994) has $r^* > 4$ m, so some caution is advised at high meter scales. Moreover, note that Bray et al. (2018) reported margin D values of ~ 1.30 – 1.35 for three lunar granular flows using the divider method (section 3.2.2) at decameter scales, and we measure margin D values in that same range at $r^* \geq 5.8$ m for HAW-09, a pāhoehoe margin.

5.3.3 Intermediate margin D

Among best-suited margin intervals on shallow slopes (generally $\lesssim 4^\circ$) in the present study, all four interval from transitional lava types have D values in the range 1.10–1.12 at some scale in $r^* = 1\text{--}10$ m, but no interval from another morphologic type has a D value in that range. For Bruno et al. (1994), and again considering only best-suited margin intervals on shallow slopes analyzed at meter scales, two of the four interval from transitional lava types have D values in the same 1.10–1.12 range, and only one mafic interval of any other morphologic type, pāhoehoe, has a D value in this range. The other 21 pāhoehoe margin intervals in that study have $D \geq 1.14$. (For completeness, we note that Bruno et al. (1994) did not specify by what criteria they determined a slope to qualify as shallow.)

We propose that for best-suited basaltic lava margins on shallow slopes, meter-scale D values of 1.10–1.12 (rounded to the nearest hundredth) are most commonly associated with transitional morphologic types (cf. Bruno et al., 1994). However, the results of Bruno et al. (1994) for non-mafic lava margin intervals suggests that caution should be taken when it is not known whether a flow is mafic. Among margin intervals of basaltic andesite, they measured D values of 1.10 and 1.13 for two of four intervals using r of 10–31.6 m and observed a trend of decreasing D values with fining scale for r of 10–4500 m. These observations suggest that non-mafic margin intervals may also be associated with meter-scale D values of 1.10–1.12, though the one example of a non-mafic margin interval from the present study, IDA-01, has lower D values (section 5.1.2). Likewise, the results in the present study for HAW-15, on a 15° slope (section 5.1.3), suggest that morphologic types with higher intrinsic meter-scale margin D values could have those values depressed into the range 1.10–1.12 by steep slopes.

5.3.4 Low margin D

Our results suggest that both ‘a’ā, as noted by Bruno et al. (1994), and some transitional lava types have intrinsic meter-scale margin $D \leq 1.09$, at least at some scales. The non-mafic IDA-01 in the present study also has $D \leq 1.09$ (rounded to the nearest hundredth) across all analyzed scales. Similarly, Bruno et al. (1994) reported margin $D \leq 1.09$ for all four intervals of dacite and rhyolite and for one of four intervals of basaltic andesite using r of 10–31.6 m (and, as noted above, observed a trend of decreasing D values with fining scale).

Nonetheless, relatively low meter-scale margin D values potentially support the exclusion of pāhoehoe for best-suited flows, subject to some caveats. As pāhoehoe has intrinsic meter-scale margin $D \geq 1.13$ (section 5.3.2), the measurement of a meter-scale margin $D < 1.13$ for a best-suited lava flow on a shallow slope would suggest that the margin is not pāhoehoe. Similarly, if the D values for systematically sampled best-suited margin intervals in a flow field or region are < 1.13 at meter scales, pāhoehoe would be unlikely to dominate in that location unless steep slopes are also abundant. This test is particularly valuable in view of the hypothesis of Self et al. (1998) that pāhoehoe is the typical morphologic type of large lava deposits.

Moreover, this statistical exclusion test may be applicable at coarser scales and possibly to other planetary surfaces. Bruno et al. (1994) measured $D \geq 1.13$ for 15 of 16 meter-scale (field) analyses of pāhoehoe margin intervals and for 7 of 7 (photographic) analyses at coarser scales. Furthermore, Bruno and Taylor (1995) analyzed margin intervals from lava flows on Venus using both margin fractal analysis and an independent classification framework based on

radar-derived surface roughness (Campbell & Campbell, 1992). For all 11 margin intervals with $D \geq 1.13$, the radar-based framework classified each as pāhoehoe or transitional.

6 Conclusions

In the field, we measured the geometry of 15 geomorphically fresh lava flow margin intervals with decimeter precision. These intervals come from Hawai‘i, Iceland, and Idaho and represent a wide variety of morphologic types. Based on multi-scale fractal analysis of these geometries, we make the following conclusions.

1. Across representative scales of ~1–10 m (i.e., meter scales), lava flow margins exhibit diverse geometric behaviors. This diversity includes empirical fractality that varies from strongly scale-dependent to relatively scale-independent, even among flows of the same morphologic type.
2. The respective fractal behaviors of pāhoehoe margins and margins of transitional lava types partially overlap at meter scales, including both effective fractal dimensions and relative scale dependence. Therefore, these types cannot always be distinguished based on margin fractal analysis alone at these scales.
3. Steep slopes and topographic confinement can strongly depress the effective fractal dimension of lava margins. Consequently, margins of morphologic types that have intrinsically low effective fractal dimensions cannot be distinguished from margins of other morphologic types at meter scales unless the topographic context at the time of the flow’s emplacement is independently constrained.
4. In view of these results, we propose a new interpretive framework for meter-scale fractal analysis of lava flow margins. Within this framework, $D \geq 1.13$ is consistent with pāhoehoe and some transitional types, and $D \geq 1.20$ strongly suggests pāhoehoe; D in the range 1.10–1.12 on shallow slopes is most commonly associated with flows of transitional lava types; and $D < 1.13$ on a shallow slope suggests that a margin is not pāhoehoe. This framework is best suited to geomorphically fresh flows that were emplaced subaerially on Earth without significant topographic confinement, but may also have value in other contexts.

Acknowledgments and Data

Work in Hawai‘i Volcanoes National Park and Craters of the Moon National Monument and Preserve was conducted under science permits HAVO-2012-SCI-0025, HAVO-2016-SCI-0047, and CRMO-2014-SCI-0004. Work at Holuhraun was conducted with permission from the Vatnajökull National Park (Vatnajökulsþjóðgarður) service. This material is based in part on work supported by the National Science Foundation Graduate Research Fellowship under Grant No. 2012116373, the University of Western Ontario, the Natural Sciences and Engineering Research Council, the Canadian Space Agency, NASA’s Solar System Exploration Research Virtual Institute (SSERVI)/Field Investigations to Enable Solar System Science and Exploration (FINESSE), a Geological Society of America Research Grant, and Dan Cavanagh. C.W.H. acknowledges support from the NASA Planetary Science and Technology from Analog Research (PSTAR) program (Grant # 80NSSC21K0011). We also thank Alfred McEwen for his valuable support, an anonymous reviewer for their comments that improved this manuscript, and Trevor

Miller, Stephen Scheidt, Youngmin JeongAhn, Xianyu Tan, and Hester Mallonee for their assistance in the field. The geometries of the 15 margin intervals and the synthetic fractals from Figure 2 are archived in this in-text reference: (Schaefer, 2020a). The Python code used to perform fractal analysis is archived in this in-text reference: (Schaefer, 2020b).

References

- Anderson, S. W., McColley, S. M., Fink, J. H., & Hudson, R. K. (2005). The development of fluid instabilities and preferred pathways in lava flow interiors: Insights from analog experiments and fractal analysis. *Geological Society of America Special Paper* 396, 2396(10), 147–161. <https://doi.org/10.1130/0-8137-2396-5.147>
- Andrle, R. (1992). Estimating fractal dimension with the divider method in geomorphology. *Geomorphology*, 5(1–2), 131–141. [https://doi.org/10.1016/0169-555X\(92\)90061-R](https://doi.org/10.1016/0169-555X(92)90061-R)
- Andrle, R. (1996a). Complexity and Scale in Geomorphology: Statistical Self-Similarity vs. Characteristic Scales. *Mathematical Geology*, 28(3), 275–293. <https://doi.org/10.1007/BF02083201>
- Andrle, R. (1996b). The west coast of Britain: Statistical self-similarity vs. characteristic scales in the landscape. *Earth Surface Processes and Landforms*, 21(10), 955–962. [https://doi.org/10.1002/\(SICI\)1096-9837\(199610\)21:10<955::AID-ESP639>3.0.CO;2-Y](https://doi.org/10.1002/(SICI)1096-9837(199610)21:10<955::AID-ESP639>3.0.CO;2-Y)
- Avnir, D., Biham, O., Lidar, D., & Malcai, O. (1998). Is the Geometry of Nature Fractal? *Science (New York, N.Y.)*, 279(5347), 39–40.
- Blake, S., & Bruno, B. . (2000). Modelling the emplacement of compound lava flows. *Earth and Planetary Science Letters*, 184(1), 181–197. [https://doi.org/10.1016/S0012-821X\(00\)00278-8](https://doi.org/10.1016/S0012-821X(00)00278-8)
- Bonnefoy, L. E., Hamilton, C. W., Scheidt, S. P., Duhamel, S., Höskuldsson, Jónsdóttir, I., et al. (2019). Landscape evolution associated with the 2014–2015 Holuhraun eruption in Iceland. *Journal of Volcanology and Geothermal Research*, 387, 106652. <https://doi.org/10.1016/j.jvolgeores.2019.07.019>
- Bray, V. J., Atwood-Stone, C., Neish, C. D., Artemieva, N. A., McEwen, A. S., & McElwaine, J. N. (2018). Lobate impact melt flows within the extended ejecta blanket of Pierazzo crater. *Icarus*, 301, 26–36. <https://doi.org/10.1016/J.ICARUS.2017.10.002>
- Bruno, B. C., & Taylor, G. J. (1995). Morphologic identification of Venusian lavas. *Geophysical Research Letters*, 22(14), 1897–1900. <https://doi.org/10.1029/95GL01318>
- Bruno, B. C., Taylor, G. J., Rowland, S. K., Lucey, P. G., & Self, S. (1992). Lava Flows are Fractals. *Geophysical Research Letters*, 19(3), 305–308. <https://doi.org/10.1029/91gl03039>
- Bruno, B. C., Taylor, G. J., Rowland, S. K., & Baloga, S. M. (1994). Quantifying the effect of rheology on lava-flow margins using fractal geometry. *Bulletin of Volcanology*, 56(3), 193–206. <https://doi.org/10.1007/BF00279604>
- Campbell, B. A., & Campbell, D. B. (1992). Analysis of volcanic surface-morphology on Venus from comparison of Arecibo, Magellan, and terrestrial airborne radar data. *Journal of Geophysical Research-Planets*, 97(E10), 16293–16314. <https://doi.org/10.1029/92JE01558>

- Cashman, K. V., Thornber, C., & Kauahikaua, J. P. (1999). Cooling and crystallization of lava in open channels, and the transition of Pāhoehoe Lava to 'A'ā. *Bulletin of Volcanology*, 61(5), 306–323. <https://doi.org/10.1007/s004450050299>
- Chowdhury, A. R., Saxena, M., Kumar, A., Joshi, S. R., Amitabh, Dagar, A., et al. (2020). Orbiter high resolution camera onboard chandrayaan-2 orbiter. *Current Science*, 118(4), 560–565. <https://doi.org/10.18520/cs/v118/i4/560-565>
- Christensen, P. R., Jakosky, B. M., Kieffer, H. H., Malin, M. C., McSween, H. Y., Neelson, K., et al. (2004). The Thermal Emission Imaging System (THEMIS) for the Mars 2001 Odyssey mission. *Space Science Reviews*. Springer. <https://doi.org/10.1023/b:spac.0000021008.16305.94>
- Christensen, P. R., McSween, H. Y., Bandfield, J. L., Ruff, S. W., Rogers, A. D., Hamilton, V. E., et al. (2005). Evidence for magmatic evolution and diversity on Mars from infrared observations. *Nature*, 436(7050), 504–509. <https://doi.org/10.1038/nature03639>
- Economou, T. (2001). Chemical analyses of martian soil and rocks obtained by the Pathfinder Alpha Proton X-ray spectrometer. In *Radiation Physics and Chemistry* (Vol. 61, pp. 191–197). Pergamon. [https://doi.org/10.1016/S0969-806X\(01\)00240-7](https://doi.org/10.1016/S0969-806X(01)00240-7)
- Evangelidis, G. D., & Psarakis, E. Z. (2008). Parametric image alignment using enhanced correlation coefficient maximization. *IEEE Transactions on Pattern Analysis and Machine Intelligence*, 30(10), 1858–1865. <https://doi.org/10.1109/TPAMI.2008.113>
- Falconer, K. (2003). *Fractal Geometry: Mathematical Foundations and Applications, Second Edition*. Wiley & Sons. <https://doi.org/10.1002/0470013850>
- Finch, R. H. (1933). Block Lava. *The Journal of Geology*, 41(7), 769–770. <https://doi.org/10.1086/624096>
- Gaonac'h, H., Lovejoy, S., & Stix, J. (1992). Scale invariance of basaltic lava flows and their fractal dimensions. *Geophysical Research Letters*, 19(8), 785–788. <https://doi.org/10.1029/92GL00545>
- Gneiting, T., & Schlather, M. (2004). Stochastic models that separate fractal dimension and the hurst effect. *SIAM Review*, 46(2), 269–282. <https://doi.org/10.1137/S0036144501394387>
- Gneiting, T., Ševčíková, H., & Percival, D. B. (2012). Estimators of fractal dimension: Assessing the roughness of time series and spatial data. *Statistical Science*, 27(2), 247–277. <https://doi.org/10.1214/11-STS370>
- Gregg, T. K. P. (2017). Patterns and processes: Subaerial lava flow morphologies: A review. *Journal of Volcanology and Geothermal Research*, 342, 3–12. <https://doi.org/10.1016/J.JVOLGEORES.2017.04.022>
- Hamilton, C. W. (2019). “Fill and spill” lava flow emplacement: Implications for understanding planetary flood basalt eruptions. In N. F. Six & G. Karr (Eds.), *Marshall Space Flight*

Center Faculty Fellowship Program (p. 9). NASA (TM—2019–220139). Retrieved from <https://ntrs.nasa.gov/archive/nasa/casi.ntrs.nasa.gov/20200000048.pdf>

Hamilton, C. W., Scheidt, S. P., Sori, M. M., Wet, A. P., Bleacher, J. E., Mougini-Mark, P. J., et al. (2020). Lava-Rise Plateaus and Inflation Pits in the McCartys Lava Flow Field, New Mexico: An Analog for Pāhoehoe-Like Lava Flows on Planetary Surfaces. *Journal of Geophysical Research: Planets*, 125(7). <https://doi.org/10.1029/2019JE005975>

Harris, A. J. L., Rowland, S. K., Villeneuve, N., & Thordarson, T. (2017). Pāhoehoe, ‘a‘ā, and block lava: an illustrated history of the nomenclature. *Bulletin of Volcanology*, 79(1), 7. <https://doi.org/10.1007/s00445-016-1075-7>

Hayward, J., Orford, J. D., & Brian Whalley, W. (1989). Three implementations of fractal analysis of particle outlines. *Computers and Geosciences*, 15(2), 199–207. [https://doi.org/10.1016/0098-3004\(89\)90034-4](https://doi.org/10.1016/0098-3004(89)90034-4)

Holcomb, R. T. (1987). Eruptive history and long-term behavior of Kilauea Volcano. In R. W. Decker, T. L. Wright, & P. H. Stauffer (Eds.), *Volcanism in Hawaii: U.S. Geological Survey Professional Paper 1350, Volume 1* (pp. 261–350).

Hon, K., Gansecki, C., & Kauahikaua, J. (2003). The Transition from ‘A‘ā to Pāhoehoe Crust on Flows Emplaced During the Pu‘u ‘Ō‘ō-Kūpaianaha Eruption. *USGS Prof. Paper 1676*, 89–103. [https://doi.org/10.1016/0003-6870\(73\)90259-7](https://doi.org/10.1016/0003-6870(73)90259-7)

Hughes, S. S., Haberle, C. W., Kobs Nawotniak, S. E., Sehlke, A., Garry, W. B., Elphic, R. C., et al. (2019). Basaltic Terrains in Idaho and Hawai‘i as Planetary Analogs for Mars Geology and Astrobiology. *Astrobiology*, 19(3), 260–283. <https://doi.org/10.1089/ast.2018.1847>

Keszthelyi, L. P. (2002). Classification of the mafic lava flows from ODP Leg 183. *Proceedings of the Ocean Drilling Program, Scientific Results*, 183(February), 1–28.

Keszthelyi, L. P., McEwen, A. S., & Thordarson, T. (2000). Terrestrial analogs and thermal models for Martian flood lavas. *Journal of Geophysical Research: Planets*, 105(E6), 15027–15049. <https://doi.org/10.1029/1999JE001191>

Keszthelyi, L. P., Thordarson, T., McEwen, A., Haack, H., Guilbaud, M. N., Self, S., & Rossi, M. J. (2004). Icelandic analogs to Martian flood lavas. *Geochemistry, Geophysics, Geosystems*, 5(11), Q11014. <https://doi.org/10.1029/2004GC000758>

Kilburn, C. R. J. (1990). Surfaces of Aa Flow-Fields on Mount Etna, Sicily: Morphology, Rheology, Crystallization and Scaling Phenomena. In J. H. Fink (Ed.), *Lava Flows and Domes: Emplacement Mechanisms and Hazard Implications* (pp. 129–156). Berlin Heidelberg: Springer-Verlag. https://doi.org/10.1007/978-3-642-74379-5_6

Kilburn, C. R. J. (1996). Patterns and predictability in the emplacement of subaerial lava flows and flow fields. In *Monitoring and Mitigation of Volcano Hazards* (pp. 491–537). Berlin Heidelberg: Springer-Verlag. https://doi.org/doi:10.1007%2F978-3-642-80087-0_15

- Kirk, R. L., Howington-Kraus, E., Rosiek, M. R., Anderson, J. A., Archinal, B. A., Becker, K. J., et al. (2008). Ultrahigh resolution topographic mapping of Mars with MRO HiRISE stereo images: Meter-scale slopes of candidate Phoenix landing sites. *Journal of Geophysical Research*, 113, E00A24. <https://doi.org/10.1029/2007JE003000>
- Klinkenberg, B. (1994). A review of methods used to determine the fractal dimension of linear features. *Mathematical Geology*, 26(1), 23–46. <https://doi.org/10.1007/BF02065874>
- Klinkenberg, B., & Goodchild, M. F. (1992). The fractal properties of topography: A comparison of methods. *Earth Surface Processes and Landforms*, 17(3), 217–234. <https://doi.org/10.1002/esp.3290170303>
- Kolzenburg, S., Giordano, D., Thordarson, T., Höskuldsson, A., & Dingwell, D. B. (2017). The rheological evolution of the 2014/2015 eruption at Holuhraun, central Iceland. *Bulletin of Volcanology*, 79(6), 45. <https://doi.org/10.1007/s00445-017-1128-6>
- Kuntz, M. A., Champion, D. E., Spiker, E. C., Lefebvre, R. H., & Mcbroomes, L. A. (1982). The Great Rift and the Evolution of the Craters of the Moon Lava Field, Idaho. *Cenozoic Geology of Idaho: Idaho Bureau of Mines and Geology Bulletin*, 26, 423–437. Retrieved from http://geology.isu.edu/Digital_Geology_Idaho/papers/B-26ch7-2.pdf
- Kuntz, M. A., Elsheimer, H. N., Espos, L. F., & Klock, P. R. (1985). *USGS Open-File Report 85-0593: Major-element analyses of latest Pleistocene-Holocene lava fields of the Snake River plain, Idaho*. Retrieved from <http://search.ebscohost.com/login.aspx?direct=true&db=geh&AN=1986-014534&site=ehost-live>
- Kuntz, M. A., Spiker, E. C., Rubin, M., Champion, D. E., & Lefebvre, R. H. (1986). Radiocarbon studies of latest Pleistocene and Holocene lava flows of the Snake River Plain, Idaho: Data, lessons, interpretations. *Quaternary Research*, 25(2), 163–176. [https://doi.org/10.1016/0033-5894\(86\)90054-2](https://doi.org/10.1016/0033-5894(86)90054-2)
- Kvålseth, T. O. (1985). Cautionary Note about R^2 . *American Statistician*, 39(4), 279–285. <https://doi.org/10.1080/00031305.1985.10479448>
- Leeman, W. P., Vitaliano, C. J., & Prinz, M. (1976). Evolved Lavas from the Snake River Plain. *Contributions to Mineralogy and Petrology*, 56, 35–60. Retrieved from <https://link-springer-com.ezproxy1.library.arizona.edu/content/pdf/10.1007%2F00375420.pdf>
- Li, M., & Li, J. Y. (2017). Generalized Cauchy model of sea level fluctuations with long-range dependence. *Physica A: Statistical Mechanics and Its Applications*, 484, 309–335. <https://doi.org/10.1016/j.physa.2017.04.130>
- Lipman, P. W., & Banks, N. G. (1987). Aa flow dynamics, Mauna Loa 1984. In R. W. Decker, T. L. Wright, & P. H. Stauffer (Eds.), *Volcanism in Hawaii: U.S. Geological Survey Professional Paper 1350, Volume 2* (pp. 1527–1567). Retrieved from <https://www.researchgate.net/publication/262261672>

- 988 Luongo, G., Mazzarella, A., & Di Donna, G. (2000). Multifractal characterization of Vesuvio
989 lava-flow margins and its implications. *Journal of Volcanology and Geothermal Research*,
990 101(3–4), 307–311. [https://doi.org/10.1016/S0377-0273\(00\)00175-X](https://doi.org/10.1016/S0377-0273(00)00175-X)
- 991 Macdonald, G. A. (1953). Pahoehoe, aa, and block lava. *American Journal of Science*, 251(3),
992 169–191. <https://doi.org/10.2475/ajs.251.3.169>
- 993 Maeno, F., Nakada, S., & Kaneko, T. (2016). Morphological evolution of a new volcanic islet
994 sustained by compound lava flows. *Geology*, 44(4), 259–262.
995 <https://doi.org/10.1130/G37461.1>
- 996 Mandelbrot, B. B. (1967). How Long Is the Coast of Britain? Statistical Self-similarity and
997 Fractional Dimension. *Science (New York, N.Y.)*, 156(3775), 636–638.
998 <https://doi.org/10.1126/science.156.3775.636>
- 999 Mandelbrot, B. B. (1982). *The Fractal Geometry of Nature*. New York: W.H. Freeman.
1000 <https://doi.org/10.2307/3615422>
- 1001 Mandelbrot, B. B. (1986). Self-affine fractal sets, II: Length and surface dimensions. In *Fractals*
1002 *in Physics* (pp. 17–20). Elsevier. <https://doi.org/10.1016/b978-0-444-86995-1.50005-6>
- 1003 Mandelbrot, B. B. (2002). *Gaussian Self-Affinity and Fractals: Globality, the Earth, 1/f Noise,*
1004 *and R/S*. New York: Springer-Verlag.
- 1005 Maria, A., & Carey, S. (2002). Using fractal analysis to quantitatively characterize the shapes of
1006 volcanic particles. *Journal of Geophysical Research: Solid Earth*, 107(B11), ECV 7-1-ECV
1007 7-17. <https://doi.org/10.1029/2001jb000822>
- 1008 Mark, D. M., & Aronson, P. B. (1984). Scale-dependent fractal dimensions of topographic
1009 surfaces: An empirical investigation, with applications in geomorphology and computer
1010 mapping. *Journal of the International Association for Mathematical Geology*, 16(7), 671–
1011 683. <https://doi.org/10.1007/BF01033029>
- 1012 McEwen, A. S., Eliason, E. M., Bergstrom, J. W., Bridges, N. T., Hansen, C. J., Delamere, W.
1013 A., et al. (2007). Mars Reconnaissance Orbiter’s High Resolution Imaging Science
1014 Experiment (HiRISE). *Journal of Geophysical Research*, 112, E05S02.
1015 <https://doi.org/10.1029/2005JE002605>
- 1016 Mitchell, N. C., Beier, C., Rosin, P. L., Quartau, R., & Tempera, F. (2008). Lava penetrating
1017 water: Submarine lava flows around the coasts of Pico Island, Azores. *Geochemistry,*
1018 *Geophysics, Geosystems*, 9(3), n/a-n/a. <https://doi.org/10.1029/2007GC001725>
- 1019 Moratto, Z., Nefian, A., Beyer, R., Hancher, M., Lundy, M., ALEXANDROV, O., et al. (2013).
1020 Ames Stereo Pipeline, NASA’s Open Source Automated Stereogrammetry Software. *Lunar*
1021 *and Planetary Science Conference*, 2364. Retrieved from
1022 <https://www.lpi.usra.edu/meetings/lpsc2010/pdf/2364.pdf>
- 1023 Moré, J. J. (1978). The Levenberg-Marquardt algorithm: Implementation and theory. In G. A.

- Watson (Ed.), *Numerical Analysis* (pp. 105–116). Springer-Verlag.
<https://doi.org/10.1007/BFb0067700>
- Neish, C. D., Hamilton, C. W., Hughes, S. S., Nawotniak, S. K., Garry, W. B., Skok, J. R., et al. (2017). Terrestrial analogues for lunar impact melt flows. *Icarus*, 281, 73–89.
<https://doi.org/10.1016/j.icarus.2016.08.008>
- Neuman, S. P., Guadagnini, A., Riva, M., & Siena, M. (2013). Recent Advances in Statistical and Scaling Analysis of Earth and Environmental Variables. In *Advances in Hydrogeology* (pp. 1–25). New York, NY: Springer New York. https://doi.org/10.1007/978-1-4614-6479-2_1
- Pedersen, G. B. M., Höskuldsson, A., Dürig, T., Thordarson, T., Jónsdóttir, I., Riishuus, M. S., et al. (2017). Lava field evolution and emplacement dynamics of the 2014–2015 basaltic fissure eruption at Holuhraun, Iceland. *Journal of Volcanology and Geothermal Research*, 340, 155–169. <https://doi.org/10.1016/J.JVOLGEORES.2017.02.027>
- Peterson, D. W., & Tilling, R. I. (1980). Transition of basaltic lava from pahoehoe to aa, Kilauea Volcano, Hawaii: Field observations and key factors. *Journal of Volcanology and Geothermal Research*, 7(3–4), 271–293. [https://doi.org/10.1016/0377-0273\(80\)90033-5](https://doi.org/10.1016/0377-0273(80)90033-5)
- Pyle, D. M., & Elliott, J. R. (2006). Quantitative morphology, recent evolution, and future activity of the Kameni Islands volcano, Santorini, Greece. *Geosphere*, 2(5), 253.
<https://doi.org/10.1130/GES00028.1>
- Richardson, L. F. (1961). The problem of contiguity: An appendix to “Statistic of Deadly Quarrels.” *General Systems: Yearbook of the Society for the Advancement of General Systems Theory*, 6, 139–187. Retrieved from <http://cds.cern.ch/record/434833>
- Rieder, R., Economou, T., Wänke, H., Turkevich, A., Crisp, J., Brückner, J., et al. (1997, December 5). The chemical composition of martian soil and rocks returned by the mobile alpha proton x-ray spectrometer: Preliminary results from the x-ray mode. *Science*. American Association for the Advancement of Science.
<https://doi.org/10.1126/science.278.5344.1771>
- Robinson, M. S., Brylow, S. M., Tschimmel, M., Humm, D., Lawrence, S. J., Thomas, P. C., et al. (2010). Lunar Reconnaissance Orbiter Camera (LROC) Instrument Overview. *Space Science Reviews*, 150(1–4), 81–124. <https://doi.org/10.1007/s11214-010-9634-2>
- Rowland, S. K., & Walker, G. P. (1990). Pahoehoe and aa in Hawaii: volumetric flow rate controls the lava structure. *Bulletin of Volcanology*, 52(8), 615–628.
<https://doi.org/10.1007/BF00301212>
- Rowland, S. K., & Walker, G. P. L. (1987). Toothpaste lava: Characteristics and origin of a lava structural type transitional between pahoehoe and aa. *Bulletin of Volcanology*, 49(4), 631–641. <https://doi.org/10.1007/BF01079968>
- Sandmeyer, E., Nawotniak, S. E. K., Hughes, S. S., Elphic, R. C., Lim, D. S. S., & Heldmann, J.

(2017). Frothy Lava At Highway Flow, Craters of the Moon. *Lunar and Planetary Science Conference*, #2838. Retrieved from <https://www.hou.usra.edu/meetings/lpsc2017/pdf/2838.pdf>

Schaefer, E. I. (2020a). Geometries of fresh lava margins and some relevant synthetic fractals. Retrieved February 17, 2021, from <https://doi.pangaea.de/10.1594/PANGAEA.925792>

Schaefer, E. I. (2020b). Scale-dependent Fractal Analysis (ver. 0.1). <https://doi.org/10.17504/protocols.io.bmm2k48e>

Self, S., Thordarson, T., Keszthelyi, L. P., Walker, G. P. L., Hon, K., Murphy, M. T., et al. (1996). A new model for the emplacement of Columbia River basalts as large, inflated Pahoehoe Lava Flow Fields. *Geophysical Research Letters*, 23(19), 2689–2692. <https://doi.org/10.1029/96GL02450>

Self, S., Keszthelyi, L. P., & Thordarson, T. (1998). The Importance of Pāhoehoe. *Annu. Rev. Earth Planet. Sci.*, 26, 81–110. <https://doi.org/10.1146/annurev.earth.26.1.81>

Shean, D. E., Alexandrov, O., Moratto, Z. M., Smith, B. E., Joughin, I. R., Porter, C., & Morin, P. (2016). An automated, open-source pipeline for mass production of digital elevation models (DEMs) from very-high-resolution commercial stereo satellite imagery. *ISPRS Journal of Photogrammetry and Remote Sensing*, 116, 101–117. <https://doi.org/10.1016/j.isprsjprs.2016.03.012>

Shenker, O. R. (1994). Fractal geometry is not the geometry of nature. *Studies in History and Philosophy of Science Part A*, 25(6), 967–981. [https://doi.org/10.1016/0039-3681\(94\)90072-8](https://doi.org/10.1016/0039-3681(94)90072-8)

Shepard, M. K., Brackett, R. A., & Arvidson, R. E. (1995). Self-affine (fractal) topography: Surface parameterization and radar scattering. *Journal of Geophysical Research*, 100(E6), 11709. <https://doi.org/10.1029/95JE00664>

Shepard, M. K., Campbell, B. A., Bulmer, M. H., Farr, T. G., Gaddis, L. R., & Plaut, J. J. (2001). The roughness of natural terrain: a planetary and remote sensing perspective. *Journal of Geophysical Research*, 106(E12), 32777–32795. <https://doi.org/10.1029/2000JE001429>

Soule, S. A., & Cashman, K. V. (2005). Shear rate dependence of the pāhoehoe-to-‘a‘ā transition: Analog experiments. *Geology*, 33(5), 361. <https://doi.org/10.1130/G21269.1>

Stout, M. Z., Nicholls, J., & Kuntz, M. A. (1994). Petrological and mineralogical variations in 2500-2000 yr B.P. Lava Flows, craters of the moon lava field, idaho. *Journal of Petrology*, 35(6), 1681–1715. <https://doi.org/10.1093/petrology/35.6.1681>

Thordarson, T. (1995). *Volatile release and atmospheric effects of basaltic fissure eruptions*. University of Hawaii, Manoa.

Thordarson, T., & Höskuldsson, Á. (2008). Postglacial volcanism in Iceland. *Jökull*, 58, 197–228.

- 1097 Tolometti, G. D., Neish, C. D., Osinski, G. R., Hughes, S. S., & Nawotniak, S. E. K. (2020).
1098 Interpretations of lava flow properties from radar remote sensing data. *Planetary and Space*
1099 *Science*, 190, 104991. <https://doi.org/10.1016/j.pss.2020.104991>
- 1100 Voigt, J. R. C., & Hamilton, C. W. (2018). Investigating the volcanic versus aqueous origin of
1101 the surficial deposits in Eastern Elysium Planitia, Mars. *Icarus*, 309, 389–410.
1102 <https://doi.org/10.1016/J.ICARUS.2018.03.009>
- 1103 Voigt, J. R. C., Hamilton, C. W., Scheidt, S. P., Steinbrügge, G., Münzer, U., Höskuldsson, Á., et
1104 al. (2017). Facies Characterization of the 2014–2015 Holuhraun Lava Flow Field from
1105 Remote Sensing Data and Field Observations. *American Geophysical Union Fall Meeting*,
1106 P31H-3796. Retrieved from
1107 <https://ui.adsabs.harvard.edu/abs/2018AGUFM.P31H3796V/abstract>
- 1108 Whelley, P. L., Richardson, J. A., & Hamilton, C. W. (2017). Lava Channel Textures in Tartarus
1109 Colles, Elysium Planitia, Mars. *48th Lunar and Planetary Science Conference, Held 20-24*
1110 *March 2017, at The Woodlands, Texas. LPI Contribution No. 1964, Id.2491*, 48. Retrieved
1111 from <http://adsabs.harvard.edu/abs/2017LPI....48.2491W>
- 1112 Wilson, L., & Head, J. W. (1994). Review and analysis of volcanic eruption to theory
1113 relationships landforms. *Reviews of Geophysics*, 32(3), 221–263.
1114 <https://doi.org/10.1029/94RG01113>
- 1115 Wolfe, E. W., Neal, C. A., Banks, N. G., & Duggan, T. J. (1988). Geologic observations and
1116 chronology of eruptive events. In E. W. Wolfe (Ed.), *The Puu Oo Eruption of Kilauea*
1117 *Volcano, Hawaii; Episodes 1 Through 20, January 3, 1983, Through June 8, 1984. USGS*
1118 *Professional Paper 1463* (pp. 1–99).
- 1119 Wroblewski, F. B., Treiman, A. H., Bhiravarasu, S., & Gregg, T. K. P. (2019). Ovda Fluctus, the
1120 Festoon Lava Flow on Ovda Regio, Venus: Not Silica-Rich. *Journal of Geophysical*
1121 *Research: Planets*, 124(8), 2233–2245. <https://doi.org/10.1029/2019JE006039>
- 1122 You, J., Kauhanen, K., & Raitala, J. (1996). Fractal properties of outflows from Venusian impact
1123 craters. *Earth, Moon and Planets*, 73(3), 195–214. <https://doi.org/10.1007/BF00115880>